SEDIMENTOLOGY the journal of the International Association of Sedimentologists

Sedimentology (2021) **68**, 2069–2096 doi: 10.1111/sed.12844

A mixed turbidite – contourite system related to a major submarine canyon: The Marquês de Pombal Drift (south-west Iberian margin)

DAVIDE MENCARONI*,† , ROGER URGELES*, ANGELO CAMERLENGHI‡, JAUME LLOPART*, JONATHAN FORD‡,§, CRISTINA SANCHEZ SERRA*,†, WILLIAM MESERVY*,†, EULÀLIA GRÀCIA*, MICHELE REBESCO‡ and NEVIO ZITELLINI¶

**Institut de Ciències del Mar (CSIC), Passeig Marítim de la Barceloneta, 37, Barcelona, 08003, Spain*

†Universitat de Barcelona, Barcelona, 08028, Spain (E-mail: mencaroni@icm.csic.es)

‡National Institute of Oceanography and Applied Geophysics - OGS, Sgonico, Trieste, 34010, Italy

§Università degli Studi di Trieste, Trieste, 34127, Italy

¶CNR-National Research Council of Italy, ISMAR-Marine Science Institute, Bologna, 40129, Italy

Associate Editor – Adam McArthur

ABSTRACT

Synchronous interaction between bottom currents and turbidity currents has been reported often in channel–levée systems where the thickness of the turbidity currents exceeds that of the levées. Such interplay between along-slope and down-slope sedimentary processes is one of the mechanisms by which 'mixed turbidite–contourite systems' can originate. However, bottom currents flow over large areas of the seafloor, including continental slopes characterized by deeply incised submarine canyons rather than channel levées. In these cases, a direct interaction between along-slope and down-slope currents is, theoretically, unlikely to take place. In this study, oceanographic, swath bathymetry, multichannel seismic data and sediment cores are used to investigate a 25 km long, 10 km wide and up to 0.5 km thick deep-sea late Quaternary deposit that sits adjacent to the north-west flank of one of the major canyons in the North Atlantic, the São Vicente Canyon, in the Alentejo Basin (south-west Iberian margin). The area receives the influence of a strong bottom current, the Mediterranean Outflow Water, which has swept the continental slope at different water depth ranges during glacial and interglacial periods. Architectural patterns and sediment characteristics suggest that this sedimentary body, named Marquês de Pombal Drift, is the result of the interaction between the Mediterranean Outflow Water (particularly during cold periods) and turbidity currents flowing along the São Vicente Canyon. Because the canyon is incised significantly deeper (*ca* 1.5 km) than the thickness of turbidity currents, an additional process, in comparison to earlier models, is needed to allow the interaction with the Mediterranean Outflow Water and transport sediment out of the canyon. In the São Vicente Canyon, and likely in other canyons worldwide, interaction of turbidity currents with contour currents requires intermediate nepheloid layers that export the finer-grained fraction of turbidity currents out of the canyon at the boundary between major water masses.

Keywords Alentejo Basin, drift, Mediterranean Outflow Water, mixed turbidite – contourite, nepheloid layers, Quaternary, submarine canyon, submarine slope stability, SW Iberia.

INTRODUCTION

The persistent action of along-slope contour currents is capable of building thick and extensive sedimentary deposits known as contourite drifts (Stow *et al.*, 2002; Rebesco & Camerlenghi, 2008; Rebesco *et al.*, 2014). Over the last few decades, examples of ancient and modern contourite drifts, showing a wide variety of grain-size distributions, sediment compositions and stratigraphic architectures, have been found worldwide in almost all continental margins (Rebesco *et al.*, 2014). Interest in such depositional systems has increased simultaneously with their use as palaeoceanographic indicators (Rebesco *et al.*, 1996; Camerlenghi *et al.*, 1997; Llave *et al.*, 2007a; Voelker *et al.*, 2014; Miramontes *et al.*, 2019) and palaeoclimatic recorders (Grützner *et al.*, 2003), and for their economic importance in the frame of hydrocarbon exploration (Viana & Rebesco, 2007; Brackenridge *et al.*, 2013; Stow *et al.*, 2013; Sansom, 2018; Fonnesu *et al.*, 2020). Recent studies also demonstrate the key role of bottom currents in the spreading and accumulation of microplastics in oceanic sediments (Kane *et al.*, 2020). Finally, the identification of contourite deposits is of paramount importance for offshore geohazard assessment (Laberg & Camerlenghi, 2008; Rebesco *et al.*, 2014; Casas *et al.*, 2015; Miramontes *et al.*, 2016a). Climatic variations modify the intensity and depth of contour current pathways, producing an alternation of poorly sorted, low-permeability, fine-grained sediments with coarser sand beds (Laberg *et al.*, 2005; Rebesco & Camerlenghi, 2006; Knutz, 2008; Miramontes *et al.*, 2016b, 2018; Brackenridge *et al.*, 2018; de Castro *et al.*, 2020; Yu *et al.*, 2020). Such alternation favours the generation of weak layers (Laberg *et al.*, 2005; Laberg & Camerlenghi, 2008; Nicholson *et al.*, 2020) and overpressure (Solheim *et al.*, 2005), which increase the likelihood of failure.

Interaction between contour currents and sediment gravity flows such as turbidity currents has been found in many areas worldwide (Rebesco *et al.*, 1996; Rasmussen *et al.*, 2003; Lucchi & Rebesco, 2007; Gong *et al.*, 2013; Edwards *et al.*, 2018; Fuhrmann *et al.*, 2020). Such interplay is recorded when there is an energy balance that allows preservation of the influence of both currents (Mulder *et al.*, 2008; Rebesco *et al.*, 2014). This is also the case in many areas within the Gulf of Cadiz, where depositional features generated by the Mediterranean Outflow Water (MOW) crossing the pathway of turbidity currents have already been documented (Mulder *et al.*, 2006; Marchès *et al.*, 2007; Hanquiez *et al.*, 2010; Brackenridge *et al.*, 2013; Alonso *et al.*, 2016; de Castro *et al.*, 2020) (Fig. 1). Previous studies have addressed the depositional architecture resulting from the interaction between contour and turbidity currents over channel–levée systems on the basis of seismic interpretation and core analysis (Shanmugam *et al.*, 1993; Rebesco *et al.*, 1996; Marchès *et al.*, 2010; Gong *et al.*, 2018; de Castro *et al.*, 2020; Fonnesu *et al.*, 2020; Fuhrmann *et al.*, 2020), as well as flume tank experiments (Miramontes *et al.*, 2020). These studies have recognized that mixed turbidite – contourite systems result in large asymmetrical levées with preferential extension in the contour-current direction (Mulder *et al.*, 2006, 2008; Rebesco *et al.*, 2007; Fonnesu *et al.*, 2020; Fuhrmann *et al.*, 2020). Examples of such contour current-influenced asymmetrical levées have been reported offshore Antarctica (Rebesco *et al.*, 1996; Michels *et al.*, 2001, 2002; Escutia *et al.*, 2002; Lucchi & Rebesco, 2007), China (Gong *et al.*, 2013), Mozambique (Fonnesu *et al.*, 2020) and Tanzania (Sansom, 2018; Fuhrmann *et al.*, 2020). All of these examples occur in channelized systems, where the depth of the incision allows overspill of turbidity currents and, hence, direct interaction with contour currents is possible. On the other hand, in canyons incised significantly deeper than the gravity flows travelling through them, such interaction so far has not been recognized. In this study, the late Pliocene to present stratigraphic architecture of the Alentejo Basin is investigated with the aim of understanding the mechanisms of interaction between contour currents (the MOW) and gravity-driven flows in heavily incised areas such as the São Vicente Canyon. In this canyon, incision is >1 km deep and thus turbidity current overspill and direct interaction with contour currents is, *a priori*, more difficult.

GEOLOGY AND OCEANOGRAPHY OF THE AREA

Tectonic setting

During the Mesozoic, the south-west Iberian margin (SWIM) underwent three different rifting stages followed by convergence that started in the Neogene lasting until the present day

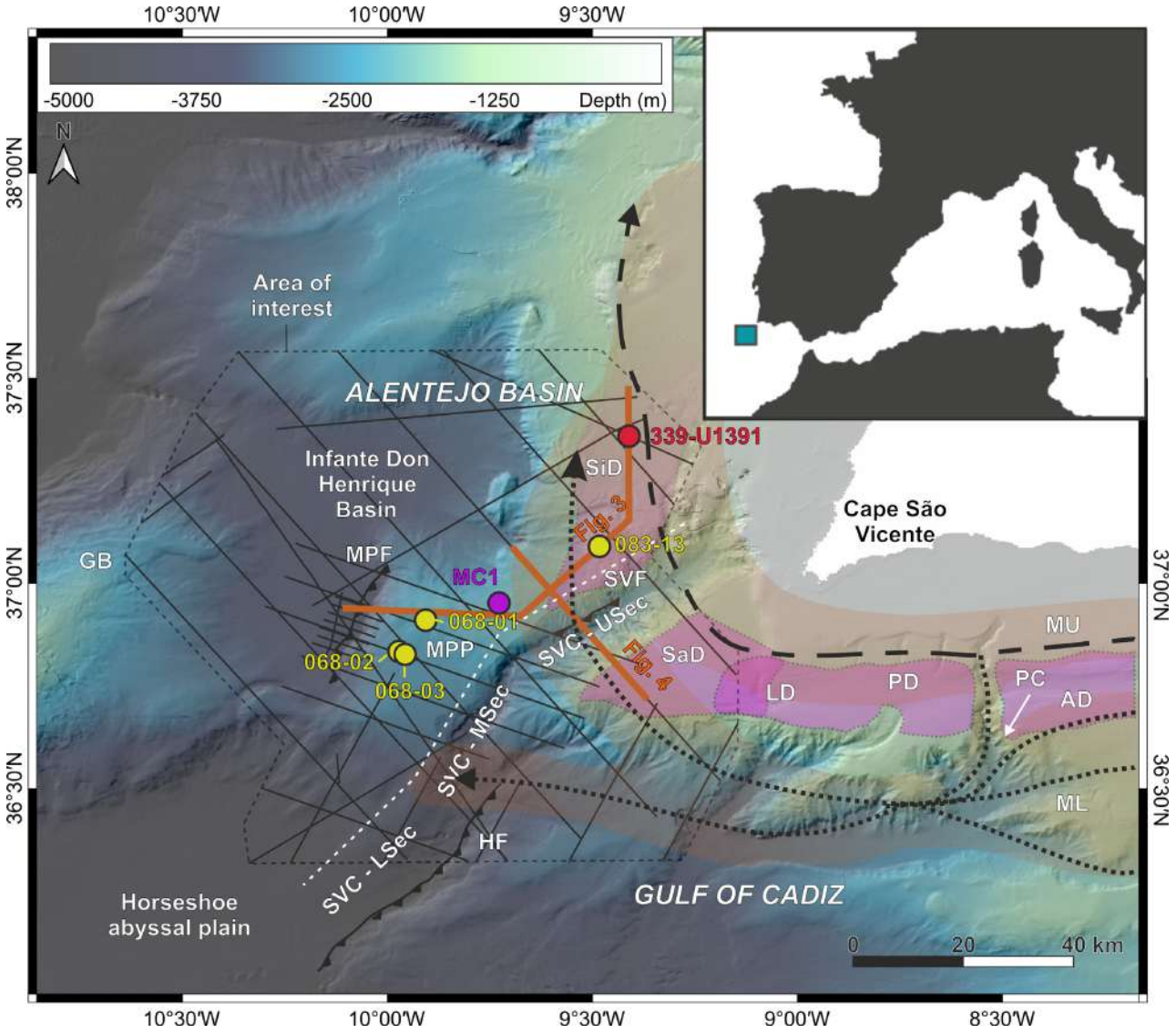

Fig. 1. Bathymetric map of Alentejo Basin and the northern part of the Gulf of Cadiz showing its main geomorphological features. Dashed arrows correspond to the main cores of the Mediterranean Outflow Water (MOW), with areas of influence shaded in red. Black lines indicate multichannel seismic (MCS) profiles used in this study. The red circle corresponds to the IODP Site U1391. Yellow circles refer to gravity cores collected during the INSIGHT Leg1 and Leg2 cruises: SdG083-13, SdG068-01, SdG068-02 and SdG068-03. The purple circle corresponds to multicore MC1 from Garcia-Orellana *et al.* (2006). Orange lines show the MCS profiles displayed in this paper (BS09 and INS2-Line10). Purple areas refer to the estimated drift depositional areas. The dashed polygon bounds the area of this study. AD: Albuera Drift; GB: Gorringe Bank; HF: Horseshoe Fault; LD: Lagos Drift; MPF: Marquês de Pombal Fault; MPP: Marquês de Pombal Plateau; MU: MOW upper core (dashed arrow); ML: MOW lower core (dotted arrow); PC: Portimão Canyon; PD: Portimão Drift; SaD: Sagres Drift; SiD: Sines Drift, SVC - LSec: São Vicente Canyon lower section; SVC – Msec: São Vicente Canyon middle section;; SVC – USec: São Vicente Canyon upper section; SVF: São Vicente Fault.

(Martínez-Loriente *et al.*, 2013, 2018; Sallarès *et al.*, 2013). The extensional north-east/south-west trending faults activated in the Mesozoic were reactivated as reverse faults and WNW–-ESE trending dextral strike-slip faults during the Neogene compression (Terrinha *et al.*, 2003, 2009; Gràcia *et al.*, 2003a,b; Zitellini *et al.*, 2009; Martínez-Loriente *et al.*, 2013, 2018; Sallarès *et al.*, 2013). South-west Iberia is an area of frequent low to intermediate magnitude

earthquakes (Mw < 5.5) (Silva *et al.*, 2017). However, it also hosts less frequent, but larger magnitude events, such as the catastrophic 1755 Lisbon earthquake (Mw > 8.5) and the more recent 1969 event (Mw 7.9 to 8) (Gràcia *et al.*, 2003a, 2010; Stich *et al.*, 2005, 2007; Baptista & Miranda, 2009; Sallarès *et al.*, 2013; Martínez-Loriente *et al.*, 2018). Earthquake ground motion is also believed to be the main trigger mechanism for the numerous Mass Transport Deposits (MTDs) recorded in the Alentejo Basin (Fig. 2) (Lebreiro *et al.*, 1997; Gràcia *et al.*, 2003b, 2010; Garcia-Orellana *et al.*, 2006; Minning *et al.*, 2006; Vizcaino *et al.*, 2006; Lo Iacono *et al.*, 2012; Urgeles & Camerlenghi, 2013).

Depositional setting

The Plio-Quaternary sedimentary history of the SWIM is strictly connected with the MOW hydrodynamic conditions and their variability through time (Stow *et al.*, 1986; Mulder *et al.*,

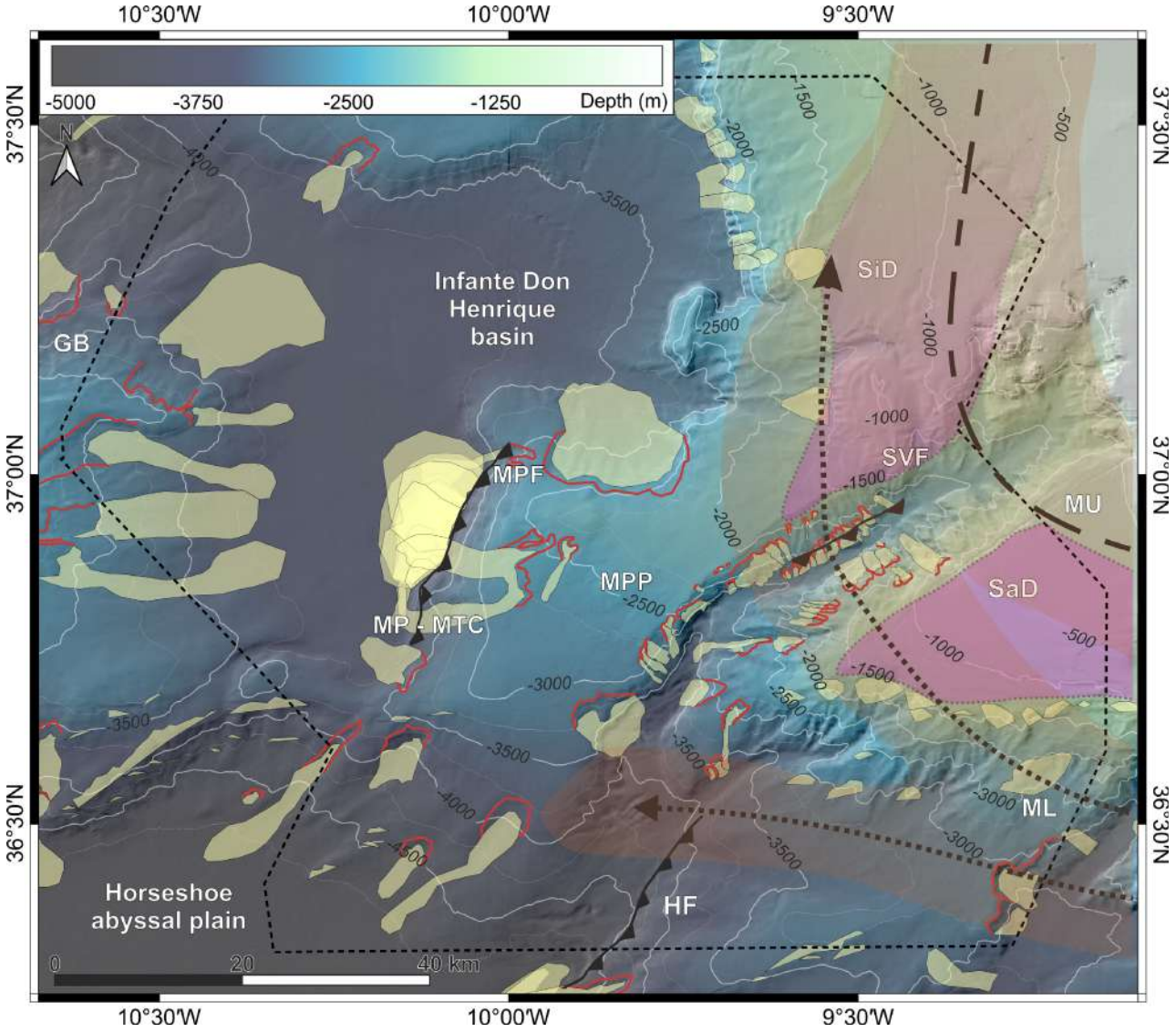

Fig. 2. Distribution of mass transport deposits (MTDs) (yellow outlines) and scars (red lines) within the area of study (dashed black outline). Dashed lines correspond to the main branches of the Mediterranean Outflow Water (MOW), with areas of influence highlighted in red. Purple areas are the estimated drift extensions. GB: Gorringe Bank; HF: Horseshoe Fault; MPF: Marquês de Pombal Fault; MPP: Marquês de Pombal Plateau; MP – MTC: Marquês de Pombal Mass Transport Complex; MU: MOW upper core; ML: MOW lower core; SaD: Sagres Drift; SiD: Sines Drift; SVF: São Vicente Fault.

2003; Llave *et al.*, 2007b, 2011; Hanquiez *et al.*, 2010; Hernández-Molina *et al.*, 2014a,b; Lofi *et al.*, 2016; Mestdagh *et al.*, 2019). An extensive contourite drift extends along the entire margin, from the Strait of Gibraltar to Cape São Vicente (Mulder *et al.*, 2003; Hernández-Molina *et al.*, 2011; Brackenridge *et al.*, 2013; Llave *et al.*, 2019) (Fig. 1). The drift consists of mixed terrigenous and biogenic sediments, where the siliciclastic fraction enters the basin through Iberian rivers, especially the Guadalquivir River (Nelson *et al.*, 1999; Mulder *et al.*, 2003; Hernández-Molina *et al.*, 2016a). The MOW transports, deposits and reworks the sediments in the SWIM, resulting in varying grain size that reflects the hydrodynamic conditions of the bottom current. Offshore Cape São Vicente the deposits are characterized by silt and mud waves, with sporadic presence of sand layers (Mulder *et al.*, 2003; Brackenridge *et al.*, 2018).

The Integrated Ocean Drilling Program (IODP) Expedition 339 acquired key geophysical and geological data along a transect, including six sites following the path of the MOW in the Gulf of Cadiz and in the Alentejo Basin (IODP Expedition 339 Scientists, 2013a; Hernández-Molina *et al.*, 2016a). Grain-size analysis and dating from the recovered cores show that contourite deposition started between 4.2 Ma and 4.5 Ma, with the coarser sediments being deposited mainly in the last 2 Myr (Fig. 3D) (Brackenridge *et al.*, 2013; Stow *et al.*, 2013; Hernández-Molina *et al.*, 2016a). Significant regional unconformities have been interpreted as periods of MOW intensification and are typically associated with local erosion, dolomite diagenesis and mass movements originating from the shallower parts of the slope (Hernández-Molina *et al.*, 2002, 2016a; Llave *et al.*, 2006, 2007a; Brackenridge *et al.*, 2013). Three main hiatuses are especially evident both in seismic profiles and from the recovered cores at 3.2 to 3.0 Ma (late Pliocene discontinuity, LPD), at 2.4 to 2.1 Ma (early Quaternary discontinuity, EQD) and at 0.8 Ma (middle Pleistocene discontinuity, MPD). A fourth, younger unconformity, more pronounced in the northern part of the Gulf of Cadiz and in the Alentejo Basin, is due to a hiatus that took place approximately between 0.4 Ma and 0.3 Ma (late Quaternary discontinuity, LQD) (Lofi *et al.*, 2016; Hernández-Molina *et al.*, 2016a) (Figs 3 and 4).

The São Vicente Canyon

The 150 km long and 20 km wide São Vicente Canyon (SVC) is the largest canyon in the SWIM and constitutes the southernmost boundary of the Alentejo Basin (Fig. 1). The development of the canyon is linked to the north-east/south-west trending São Vicente, Horseshoe and Marquês de Pombal thrust faults, which evolved under the influence of the present day African–Eurasian plate convergence (Zitellini *et al.*, 2001; Terrinha *et al.*, 2003; Gràcia *et al.*, 2003b; Bartolome *et al.*, 2012; Martínez-Loriente *et al.*, 2013, 2018). Motion of the two thrust faults since the late Miocene generated a syncline fold in between them that triggered retrogressive erosion (Serra *et al.*, 2020). The incision of the canyon developed mainly during the late Quaternary and it is nowadays still in progress, transferring sediments from the canyon upper reaches to the Horseshoe Abyssal Plain at almost 5000 m water depth (Lebreiro *et al.*, 1997; Serra *et al.*, 2020). In its present day configuration, the canyon head is located 200 metres below sea level (mbsl) and is bounded by the Sagres Drift on its southern side and the Sines Drift on its northern one (Figs 1 and 2). Based on the orientation of its longitudinal axis, the canyon can be subdivided into: (i) upper section (between 200 m and 3200 m water depth); (ii) central section (3200 to 4400 m); and (iii) lower section (4400 to 4900 m) (Serra *et al.*, 2020) (Fig. 1). Incision is deeper in the upper section and clearly asymmetrical between the two flanks: the south-east flank is steeper and incised up to 1700 m, while the north-west flank dips more gently and the incision reaches *ca* 1100 m. The shallower part of the central section shows similar asymmetry, while the deeper parts of the central section and the lower section display reversed asymmetry, with the north-west flank incised up to 880 m and the south-east flank up to 750 m (Serra *et al.*, 2020).

Numerous landslide scars located at the canyon flanks, especially in the north-west upper sector, suggest intense mass wasting activity within the SVC (Fig. 2). These mass wasting processes favour the occurrence of turbidity currents travelling along the canyon axis (Serra *et al.*, 2020). Because the canyon extends significantly into the continental shelf, many turbidity currents could also be generated at the shelf edge. Piston cores collected in the Horseshoe

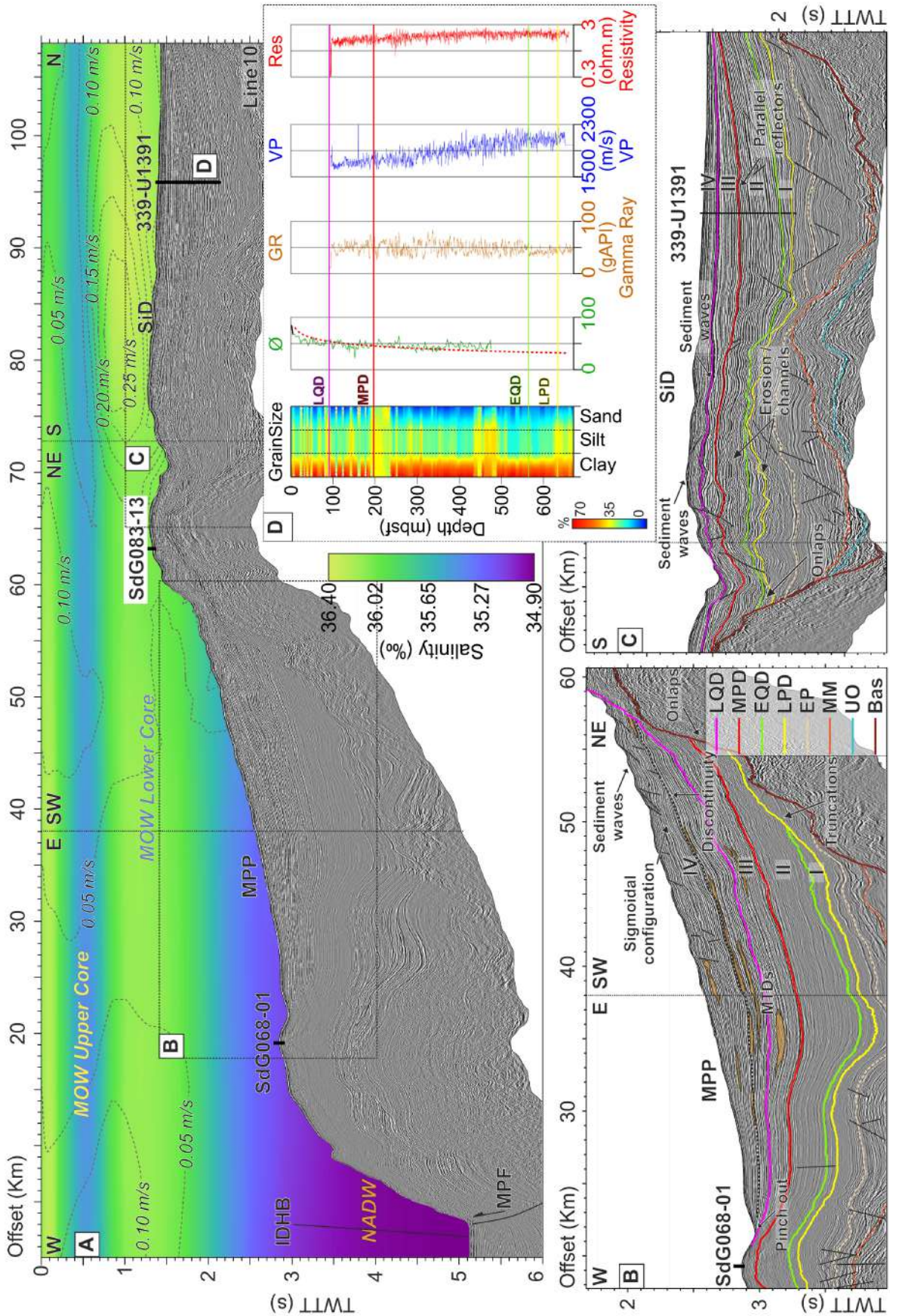
Offset (Km)
TWTT (s)
W
E
SW
NE
S
N
A
B
C
D
MOW Upper Core
MOW Lower Core
0.10 m/s
0.05 m/s
0.15 m/s
0.20 m/s
0.25 m/s
SdG083-13
SdG068-01
339-U1391
SiD
Line10
MPP
IDHB
NADW
MPF
Salinity (‰)
36.40
36.02
35.65
35.27
34.90
GrainSize
Sand
Silt
Clay
Depth (mbsf)
LQD
MPD
EQD
LPD
GR
Gamma Ray
VP
Res
Resistivity
(gAPI)
(m/s)
(ohm.m)
Sediment waves
Onlaps
Discontinuity
Sigmoidal configuration
Truncations
Pinch-out
MTDs
Erosional channels
Parallel reflectors
LQD
MPD
EQD
LPD
EP
MM
UO
Bas

Fig. 3. (A) Uninterpreted multi-channel seismic profile INS2-Line10 (see location in Fig. 1) with associated water salinity values (colour scale). Dashed grey contours indicate the computed water speed (Sotillo *et al.*, 2015; Amo *et al.*, 2020) (see *Oceanographic data* section for information about the data). (B) and (C): details of the profile, with interpretation of the main stratigraphic features. Stratigraphic interpretation follows criteria set by Hernández-Molina *et al.* (2016a) and Serra *et al.* (2020). LQD: late Quaternary discontinuity (0.4 to 0.3 Ma); MPD: middle Pleistocene discontinuity (0.8 Ma); EQD: early Quaternary discontinuity (2.4 to 2.1 Ma); LPD: late Pliocene discontinuity (3.2 to 3.0 Ma); EP: early Pliocene; MM: middle Miocene; UO: upper Oligocene; Bas: Basement. Orange bodies are MTDs. (D) Grain-size distribution and borehole logs from IODP Site U1391 (IODP Expedition 339 Scientists, 2013b). Ø (green line): porosity; GR (orange line): gamma ray log; VP (blue line): compressional velocity. IDHB: Infante Don Henrique Basin; MPF: Marquês de Pombal Fault; MPP: Marquês de Pombal Plateau; SiD: Sines Drift; 339-U1391: IODP Site U1391 location; SdG083-13 and SdG068-01: gravity cores locations; I, II, III and IV correspond to the different units defined in between the major discontinuities; vertical dashed lines correspond to the change in direction of the line (Fig. 1); vertical exaggeration *ca* 7.

Abyssal Plain (Fig. 1) reveal thick Quaternary turbidites alternating with thin hemipelagic sediments covering the entire abyssal plain (Lebreiro *et al.*, 1997; Gràcia *et al.*, 2010). This suggests that the turbidity currents generated within the SVC are able to travel the entire 356 km length of the Horseshoe Abyssal Plain, from the mouth of the SVC to its westernmost end.

Oceanographic setting

Three major water masses are present in the SWIM: the Atlantic Inflow Water (AIW), the Mediterranean Outflow Water (MOW) and the North Atlantic Deep Water (NADW) (Figs 3 and 4). The AIW is the shallowest current, and flows southward entering the Mediterranean Sea (Thorpe, 1975; Serra *et al.*, 2005). In the proximity of the Strait of Gibraltar, the AIW is characterized by high temperatures (12 to 16°C) and moderate salinities (34.7 to 36.25‰) (Llave *et al.*, 2006). Flowing below the AIW, the MOW is a current generated by the warm (13°C average temperature) and saline (37.2‰ average salinity) waters from the Mediterranean Sea that leave the Strait of Gibraltar, deflect to the west due to the Coriolis force and flow northward along the Atlantic continental slope of the Iberian Peninsula (Fig. 1). The onset of the MOW began with the opening of the Gibraltar gateway, 5.3 Ma, and gradually increased to become a major contributor to the North Atlantic oceanic circulation in the late Pliocene (Hernández-Molina *et al.*, 2014b). Since then, it has had a major influence on the sedimentation of the entire SWIM, generating one of the most extensive contourite depositional systems in the world (Ambar *et al.*, 1976; Ambar & Howe, 1979; Hernández-Molina *et al.*, 2002; Mulder *et al.*, 2003; Hanquiez *et al.*, 2007; Llave *et al.*, 2007a). The velocity of the MOW varies from 2.5 ms^{-1} at the Strait of Gibraltar, where the gateway narrows the current to a width of approximately 10 km (Baringer & Price, 2002; Mulder *et al.*, 2003; Hernández-Molina *et al.*, 2016a), to <0.2 ms^{-1} off Cape São Vicente (Johnson *et al.*, 2002; Mulder *et al.*, 2003) (Figs 3 and 4). While moving northward, the MOW flows above the colder (3 to 8°C) and less saline (34.95 to 35.2‰) NADW (Llave *et al.*, 2006; Hernández-Molina *et al.*, 2014a), a current that flows from the Greenland–Norwegian Sea region southward. The MOW begins to raft above the NADW in correspondence with Cape São Vicente, where it reaches a neutral buoyancy and detaches from the seabed (Ambar & Howe, 1979; Hernández-Molina *et al.*, 2016a).

The complex seafloor morphology of the SWIM, dominated by a set of continuous crests and troughs, diapirs and canyons, transforms the MOW single-stream, dense overflow into a multicored saline plume. Distinct channels located in the upper and mid-slope constrain spreading of the MOW and promote the formation of several MOW branches, that travel with velocity, salinity and density values that increase with depth (Sánchez-Leal *et al.*, 2017). The two major MOW pathways that are generally distinguished in the literature are the MOW upper core (MU), warmer and less saline, that flows between 500 m and 800 m, and the deeper MOW lower core (ML), flowing between 800 m and 1500 m (Fig. 1) (Ambar & Howe, 1979; Cacho *et al.*, 2000; Mulder *et al.*, 2003; Serra *et al.*, 2005). The differentiation between the upper and lower core is most likely directly inherited from the two water masses exiting the Mediterranean Sea: the Western Mediterranean

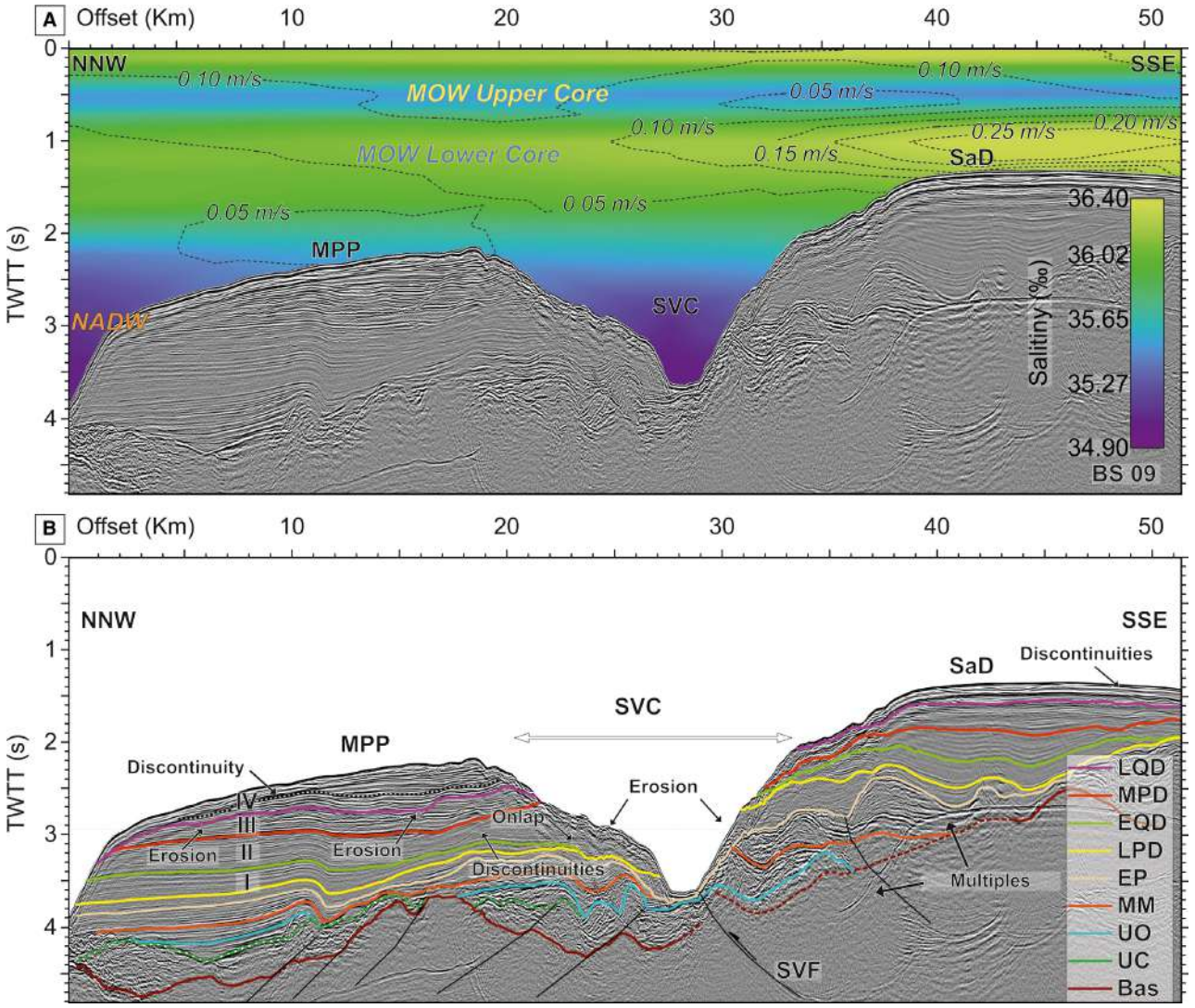

Fig. 4. (A) Uninterpreted multi-channel seismic (MCS) profile BS09 (see location in Fig. 1) with associated water salinity values (colour scale). Dashed grey contours indicate the computed water speed (Sotillo *et al.*, 2015; Amo *et al.*, 2020). (B) Interpreted MCS profile. LPD: Stratigraphic interpretation follows criteria set by Hernández-Molina *et al.* (2016a) and Serra *et al.*, (2020). LQD: late Quaternary discontinuity (0.4 to 0.3 Ma); MPD: middle Pleistocene discontinuity (0.8 Ma); EQD: early Quaternary discontinuity (2.4 to 2.1 Ma); LPD: late Pliocene discontinuity (3.2 to 3.0 Ma); EP: early Pliocene; MM: middle Miocene; UO: upper Oligocene; UC: upper Cretaceous; Bas: Basement. Orange bodies are mass transport deposits (MTDs). I, II, III and IV correspond to the different units defined in between the major discontinuities; Bas: Basement; MPP: Marquês de Pombal Plateau; SaD: Sagres Drift; SVC: São Vicente Canyon; SVF: São Vicente Fault; vertical exaggeration *ca* 4; TWTT : two-way travel time.

Deep Water (WMDW) and, especially, the Levantine Intermediate Water (LIW) (Rogerson *et al.*, 2012a; Hernández-Molina *et al.*, 2014a; Sánchez-Leal *et al.*, 2017). Seasonal climatic variations and longer term changes (for example, glacial and interglacial cycles) influence the production of the LIW. During cold periods, lower water temperatures and reduced freshwater input into the Mediterranean Basin (Bahr *et al.*, 2015) increase the density of the current exiting the Strait of Gibraltar, resulting in an enhanced ML circulation and favouring periods of sand deposition or erosion. On the other hand, higher Mediterranean water temperatures during interglacial periods, such as at present, favour a more vigorous MU circulation in the upper slope (Rogerson *et al.*, 2005; Hernández-Molina *et al.*, 2014b; Jiménez-Espejo *et al.*, 2015).

DATA AND METHODS

Geophysical data

This study is based on swath-bathymetry, two-dimensional multi-channel seismic (MCS) reflection profiles, four gravity cores, one shallow multicore (Garcia-Orellana *et al.*, 2006) and borehole data from IODP Site U1391 (Fig. 1) (IODP Expedition 339 Scientists, 2013a,b; Hernández-Molina *et al.*, 2016a). The SWIM bathymetric data is a multibeam echosounder bathymetry compilation collected during 20 marine cruises that were carried out between 2001 and 2009 (Zitellini *et al.*, 2009).

Thirty-five MCS profiles were used for this study (Fig. 1). The lines were acquired with different configurations during multiple marine surveys: (i) the ARRIFANO survey took place with the *R/V OGS EXPLORA* in 1992 (acquisition data and processing parameters reported in Zitellini *et al.* (1999), Zitellini *et al.* (2009); (ii) the BIGSETS survey carried out in 1998 onboard the *R/V URANIA* (Zitellini *et al.*, 2001, 2004); (iii) the PD00 survey acquired by TGS-NOPEC in 2000 (Llave *et al.*, 2011; Brackenridge *et al.*, 2013); (iv) the 2002 VOLTAIRE survey onboard the *R/V URANIA* (Terrinha *et al.*, 2009); (v) the INISIGHT Leg1 (2018) and Leg2 (2019) cruises, carried out with the *R/V Sarmiento de Gamboa* (Ford *et al.*, 2021).

Stratigraphic interpretation of the network of MCS profiles has been carried out using the 'IHS Kingdom Suite' seismic interpretation package. Time to depth conversion was performed to generate the thickness and sedimentation rate maps. The interval velocity model assumed a constant water velocity and a linear velocity gradient with depth below the seafloor. The model parameters were calibrated at IODP Site U1391 (IODP Expedition 339 Scientists, 2013b) using the major discontinuities of the area proposed by Hernández-Molina *et al.* (2016) (Fig. 3D) (LPD, EQD, MPD and LQD). The water velocity was set to 1514 ms^{-1} and the sediment velocity gradient was 491 ms^{-2}, derived using the measured depth and two-way travel time (TWTT) of the seafloor and LPD (deepest) horizon. The mismatch between the computed depths and the measured depth from the borehole using this gradient was <15 m for the deepest considered reflection. The seismo-stratigraphic interpretation in this study focused on the Plio-Quaternary sequence. The main depositional discontinuities described by Hernandez-Molina *et al.* (2016a). for the Sines Drift have been tracked along the available MCS network. Further to the work by Hernández-Molina *et al.* (2016a), the interpretation presented here is also based on the work by Serra *et al.* (2020) and Martínez-Loriente *et al.* (2013), which focuses on the Lower Cretaceous to Plio-Quaternary sequence in the deeper sectors of the margin. In this study, the seismic units are named sequentially from bottom to top and are bounded by the major erosional/non-depositional discontinuities identified by Hernández-Molina *et al.* (2016a).

To determine sedimentation rates, the absolute ages assigned to the considered regional discontinuities are taken from Hernández-Molina *et al.* (2016a) and Lofi *et al.* (2016) (Figs 5 and 6). Sedimentation rates here presented (Fig. 6) refer to the normalized decompacted thickness of a sedimentary unit or, in other words, the depositional thickness prior to compaction, divided by the time needed for the unit to deposit. This approach allows a more accurate comparison between older units, which have undergone more compaction relative to younger (less compacted) sediments (Llopart *et al.*, 2019). Decompacted thickness of the units has been calculated using Van Hinte's equation (Van Hinte, 1978):

$$H_i = H_f \frac{(1-\emptyset_f)}{(1-\emptyset_o)}$$

where $\emptyset_o$ is the initial porosity at deposition, $\emptyset_f$ is the present day porosity and H_f is the present day sediment thickness. $\emptyset_o$ is estimated equal for all the units and corresponds to the shallowest porosity value measured (70.4% at 0.58 m). $\emptyset_f$ is the average porosity for each of the four units at present extrapolated from IODP Site U1391 (Fig. 3D).

Grain-size and multi-sensor core logger analysis

Four gravity cores collected during the INSIGHT-Leg1 cruise in 2018 (see also Mencaroni *et al.*, 2020) and Leg2 in 2019 (Table 1; Figs 1 and 7) are analyzed un this study. Core SdG083-13 was located on the northern flank of the SVC, between the Sines Drift and the Marquês de Pombal Plateau (MPP). Cores SdG068-1, SdG068-2 and SdG068-3 were also collected within the Marquês de Pombal

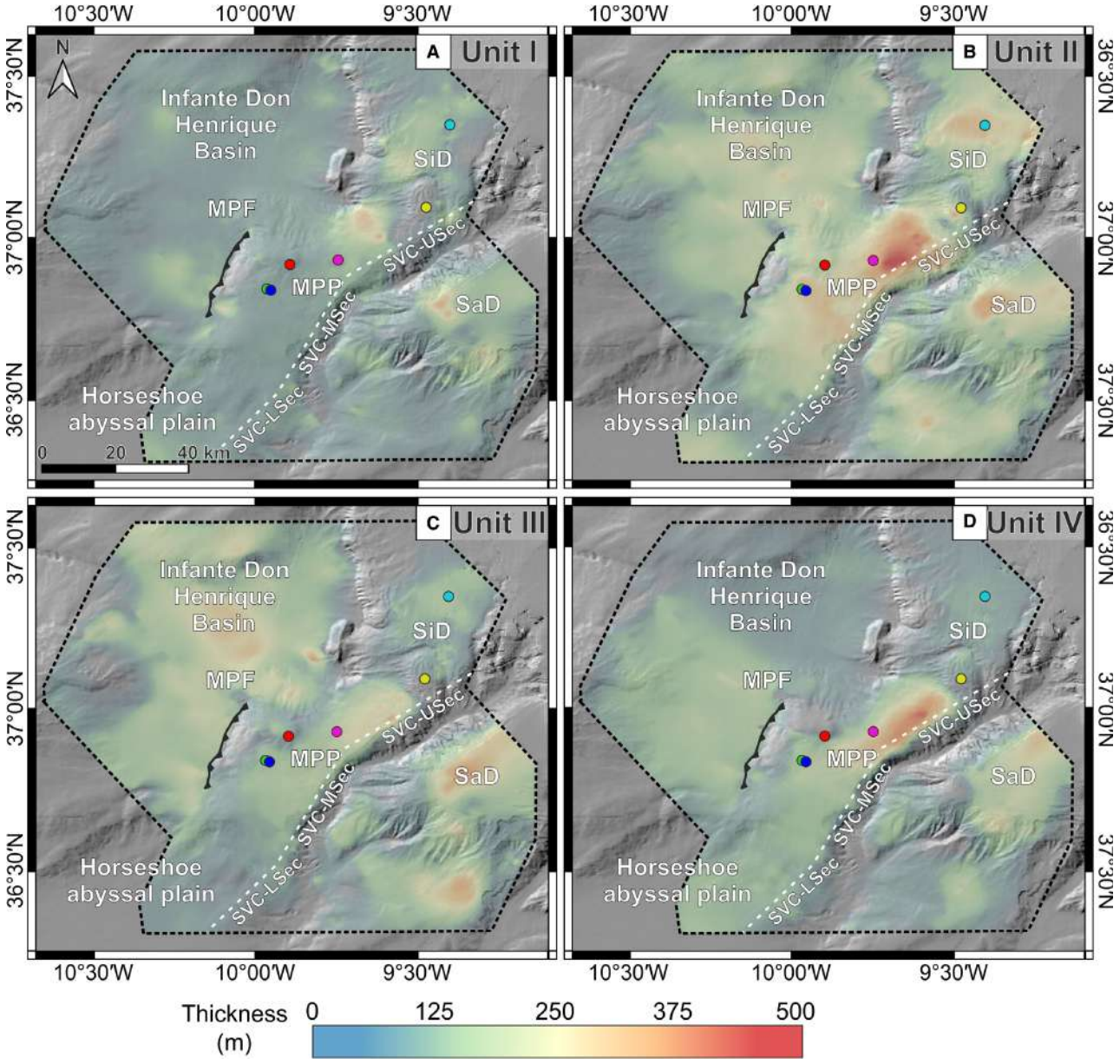

Fig. 5. Thickness distribution maps. (A) Unit I; (B) Unit II; (C) Unit III; (D) Unit IV. MPF – Marquês de Pombal Fault; MPP – Marquês de Pombal Plateau; SaD – Sagres Drift; SiD – Sines Drift; SVC – LSec: São Vicente Canyon lower section; SVC – Msec: São Vicente Canyon middle section; SVC – USec: São Vicente Canyon upper section; coloured dots indicate the location of IODP Site U1391 (light blue), multicore MC1 (red) and gravity cores SdG083-13 (yellow), SdG068-01 (red) SdG068-03 (blue) and SdG068-02 (green).

Plateau, but in deeper water (Table 1, Fig. 1). The sediments were recovered using a 5 m long, 7 cm inner diameter gravity corer weighing *ca* 800 kg.

P-wave velocity and gamma-density (Fig. 7) were measured on the whole cores with a Geotek® multi-sensor core logger (MSCL; Geotek Limited, Daventry, UK) at 0.5 cm intervals (see Frigola *et al.*, 2015). Once split, Core SdG083-13 was sampled for measurement of grain-size distribution on bulk sediment at 5 cm spacing for the whole length. Cores SdG068-1, SdG068-2 and SdG068-3 have been sampled for grain-size measurements only at specific depth intervals (Table 1) because the rest of the core was preserved unsplit for additional geotechnical tests.

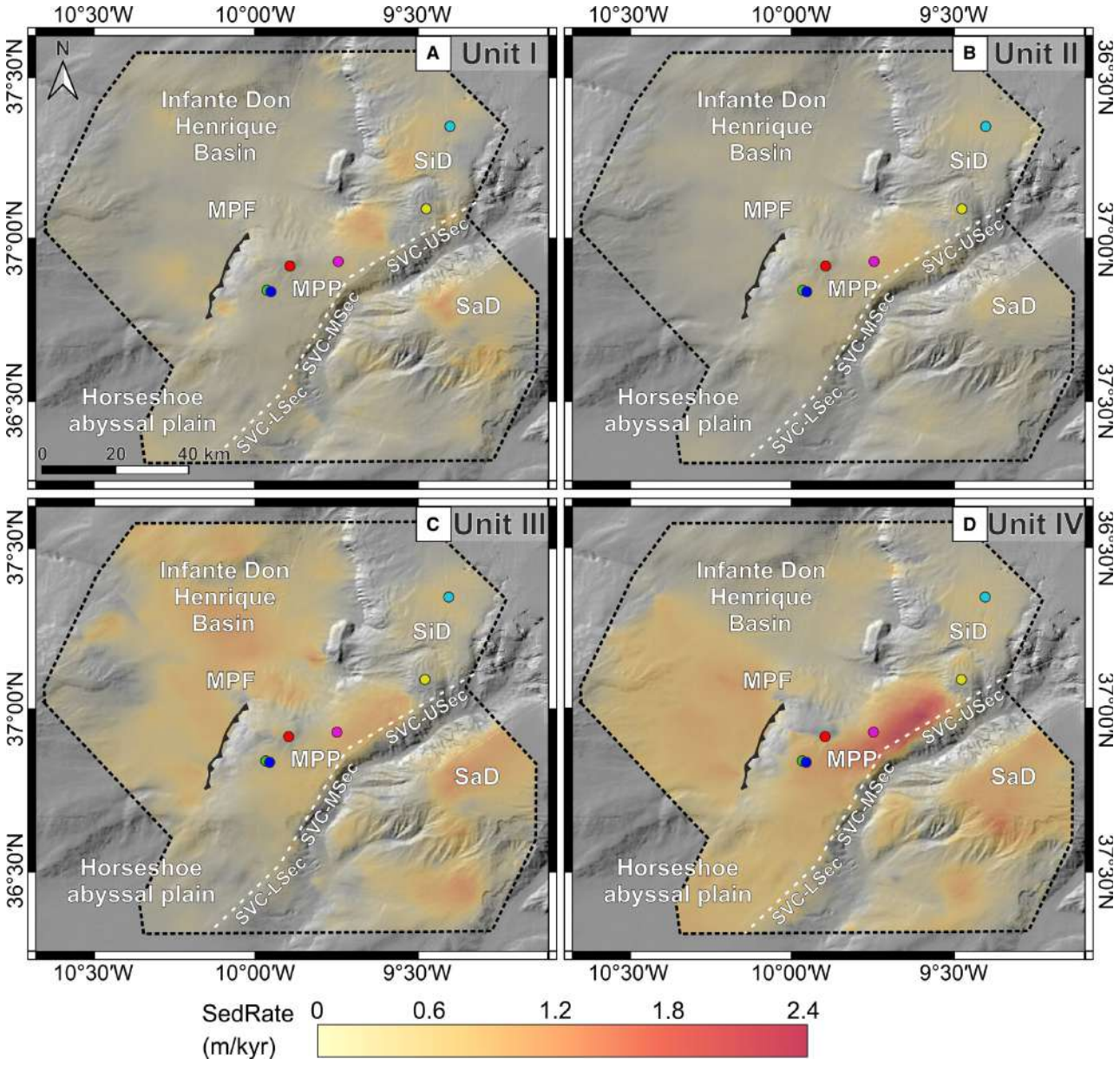

Fig. 6. Decompacted sedimentation rate maps. (A) Unit I; (B) Unit II; (C) Unit III; (D) Unit IV. MPF – Marquês de Pombal Fault; MPP – Marquês de Pombal Plateau; SaD – Sagres Drift; SiD – Sines Drift; SVC – LSec: São Vicente Canyon lower section; SVC – Msec: São Vicente Canyon middle section; SVC – USec: São Vicente Canyon upper section; coloured dots indicate the location of IODP Site U1391 and gravity cores (see Fig. 5 caption for key to colors).

Grain-size distribution for all samples was measured using a Horiba LA950 Laser Diffraction particle size analyzer (Horiba Scientific, Kyoto, Japan) for the grain-size fraction <2 mm, while the fraction >2 mm was sieved and weighted. The results obtained with the laser diffractometer were converted to percent weight and combined with those of the sieves. The grain-size classification proposed by Wentworth (1922) has been adopted (Fig. 7E).

The IODP Site U1391 (Fig. 1) drilled in 2012 recovered more than 670 m of sediments that have since been defined in terms of percentage of sand, silt and clay through smear slide

Table 1. Information on the cores used for this study.

Core	Cruise	Year	Recovery (cm)	Depth (m)	Latitude (°)	Longitude (°)	Coring system	Sample intervals (cm)
MC1	HITS-01	2001	20	2173	36.93	−9.75	Multicore	Whole core
SdG068-01	INSIGHT-Leg1	2018	243	1703	36.92	−9.90	Gravity core	180 to 195
SdG068-02	INSIGHT-Leg1	2018	215	2668	36.84	−9.97	Gravity core	78 to 110 204 to 211
SdG068-03	INSIGHT-Leg1	2018	248	2664	36.84	−9.95	Gravity core	133 to 148 240 to 248
SdG083-13	INSIGHT-Leg2	2019	236	1026	37.09	−9.48	Gravity core	Whole core

analysis (Fig. 3D) (IODP Expedition 339 Scientists, 2013c). Amongst other measurements, downhole gamma ray, density, compressional velocity and resistivity logs were acquired at the well location (Fig. 3D) (IODP Expedition 339 Scientists, 2013b; Lofi *et al.*, 2016; Hernández-Molina *et al.*, 2016a). Finally, the information provided by the 20 cm long multicore MC1, recovered during the HITS-01 cruise in 2001 in the Marquês de Pombal Plateau (Garcia-Orellana *et al.*, 2006) has been taken into account (Table 1; Figs 1 and 7). Besides other analysis, these authors constrained the sediment ages by ^{137}Cs and ^{210}Pb chronology and studied the mineral composition of the bulk and coarse fractions (>50 μm) by X-ray scans and diffraction.

Oceanographic data

Present-day water speed and salinity data discussed in this study (Figs 3A and 4; Appendix S1) are part of the Iberia–Biscay–Ireland Monitoring and Forecasting Centre (CMEMS IBI-MFC) forecast product (https://marine.copernicus.eu/) (Sotillo *et al.*, 2015; Amo *et al.*, 2020). The data refer to the monthly mean dataset of February 2020, as winter conditions reflect the present-day maximum sediment mobilization capacity of the MOW (Rogerson *et al.*, 2012b; Bahr *et al.*, 2015). The 50 depth levels present a resolution decreasing from approximately 1 m in the shallowest 10 m of water column, to more than 400 m in the deep ocean (Amo *et al.*, 2020). The seawater velocity has been computed as:

$$Ws = \sqrt{u^2 + v^2}$$

where *Ws* is the computed water speed, *u* and *v* are the eastward and northward seawater velocity components, respectively.

RESULTS

Seismic stratigraphy

The seismo-stratigraphic analysis is mainly based on the MCS profiles collected around the canyon system. The overall Plio-Quaternary stratigraphy of the area is characterized by a general increase in the amplitude of seismic reflections upward, and a general decrease in the continuity of reflections throughout the entire sequence (Figs 3 and 4). Reflection configurations evolve from parallel, in the deeper part of the study area, to sigmoidal in the shallower segments (Fig. 4B). The sequence contains several discontinuities and hiatuses characterized by truncations and onlap surfaces. A structural high in the upper reaches of the slope immediately north of the SVC (Fig. 3A) separates the MPP (Fig. 3B) from the Sines Drift (Fig. 3C).

Major discontinuities

In the Sines Drift area, the LPD appears as a laterally continuous clear erosive surface that truncates the underlying units and displays a number of channels (Fig. 3C). The LPD onlaps the structural high located on the upper reaches of the slope to the west of the SVC (Fig. 3A and C). South-west of the structural high (Fig. 3B), in the MPP (Fig. 1), the LPD does not display the same erosive character as on the location of IODP Site U1391. Here the LPD is conformable with the underlying reflections, except in close proximity to the structural high, where it truncates the older units (Fig. 3B). The LPD can also be tracked to the slope SSE of the canyon, where erosional features are present, especially in the external and shallower parts of the line (Fig. 4B). The SVC incises deeply into the LPD.

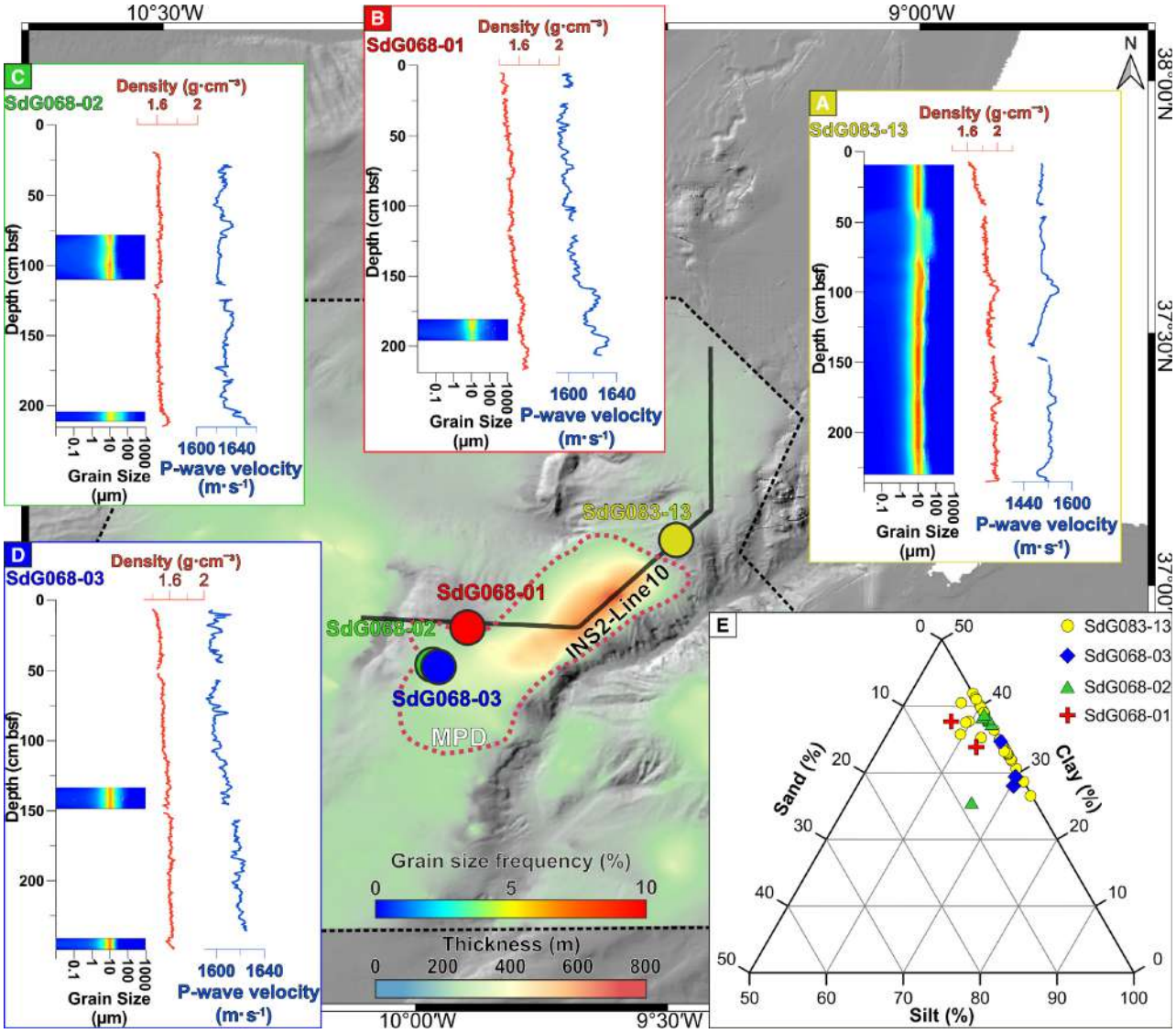

Fig. 7. Location, grain-size distribution, multi-sensor core logger (MSCL) gamma ray densities (red lines) and P-wave velocities (blue lines) of gravity cores collected for this study plotted with Unit IV thickness distribution. Red dashed outline shows the approximate areal distribution of the Marquês de Pombal Drift (MPD). (A) SdG083-13, yellow circle; (B) SdG068-01, red circle; (C) SdG068-02, green circle; (D) SdG068-03, blue circle. (E): Ternary diagram showing percentages of sand, silt and clay components for the different cores.

In the Sines Drift area, the EQD is the more prominent erosive surface and appears as a high amplitude reflection that truncates the underlying unit. The EQD also onlaps the structural high south of the Sines Drift (Fig. 3C). It is also present in the MPP, where it is conformable with the underlying reflections and onlaps the LPD towards the north-west (Fig. 3B). On the slope SSE of the SVC, the EQD appears relatively conformable with the underlying reflections and gets truncated by the canyon, while in the north-west flank, it onlaps the LPD (Fig. 4B).

As with the previous discontinuities, the MPD also appears as an erosional surface truncating the underlying horizons, especially in the proximity of the structural high on the slope north-west of the SVC (Fig. 3C). On the MPP, still on the slope north-west of the SVC, the MPD is conformable with the underlying reflections (Fig. 3B).

Unlike the deeper discontinuities, the LQD is not present in the proximity of the Marquês de Pombal thrust fault as it is truncated by the seafloor over the fault related anticline (Fig. 3B). The LQD is a clearly recognizable discontinuity in the MPP (Fig. 4B), where reflections of the topmost unit onlap.

Seismic units

The LPD, EQD, MPD and LQD discontinuities define four seismic units named I to IV from bottom to top, deposited from late Pliocene to the present day (Fig. 3D).

Unit I is bounded by the LPD at its base and the EQD at its top. This unit is characterized by middle to high frequency and high-amplitude reflections in the Sines and Sagres Drift areas. It is eroded by the EQD at the top (Figs 3C and 4B). In the shallower parts of the basin, internal erosive features such as truncations and channels characterize the unit. On the other hand, Unit I in the MPP displays relatively high-frequency, sub-parallel, low-amplitude reflections where internal erosive features are not evident (Fig. 3B). Unit I has relatively constant thickness of less than 100 m in most of the area of interest (Fig. 5A). Localized areas of erosion/non deposition are present on top of the structural highs along the most pronounced slope areas (for example, the Marquês de Pombal slope) and within the SVC. Depocentres develop on the Sagres and Sines drifts, where sediment thickness is up to 300 m (Figs 3, 4 and 5A). Unit I is also relatively thick at the footwall of the Marquês de Pombal Fault, where it can reach a thickness of more than 150 m (Figs 3B and 5A).

Unit II, bounded by EQD at its bottom and the MPD at its top, is characterized by sediment waves and internal erosional surfaces (Figs 3C and 4B). In the Sines and Sagres Drift areas, Unit II is characterized by high-frequency and continuous internal reflections. The thickness of Unit II (Fig. 5B) is more variable than that of Unit I (Fig. 5A). The average unit thickness in the Infante Don Henrique Basin is between 150 m and 250 m, while in the slope north-west of the SVC (Marquês de Pombal Plateau) it exceeds 500 m. Other depocentres include the Sines Drift, located close to IODP Site 339-U1391, where the thickness reaches 300 m, and the Sagres Drift, where the thickness reaches 350 m (Figs 3C, 4B and 5B). In the Sines Drift, Unit II is the thickest of the four units (Fig. 5B).

Unit III (Fig. 5C) is bounded by the MPD and LQD. In the Sines Drift area, the unit shows high amplitude, medium-frequency and parallel internal reflections (Fig. 3C). Towards the structural high, the unit displays large sediment waves up to 70 m high and 3.5 km in wavelength, which are separated by minor, internal erosional surfaces (Fig. 3A and C). In the proximity of the structural high, the reflections adopt complex geometries, indicating a higher energy environment, and chaotic and transparent facies associated with MTDs (Fig. 3). In the Marquês de Pombal Plateau, the reflections show weaker-amplitude close to its base (EQD), changing to stronger reflections in its upper part, where transparent lenses (MTDs) are also present (Fig. 3B). Unit III is relatively thick (up to 300 m) in the Infante Don Henrique Basin and on the slope north-west of the SVC (Fig. 5C). The main depocentre, however, is present in the Sagres Drift (400 m) and, to a lesser extent, in the MPP, the slope north-west of the SVC (up to 320 m) (Figs 3B, 4B and 5C).

Unit IV is the latest sedimentary unit, bounded by the LQD at its bottom and the Present seafloor (Fig. 5D). Similar to Unit III, in the Sines Drift, Unit IV is often characterized by high-amplitude, high-frequency and parallel reflections, changing to long sediment waves (3 km wavelength) and internal unconformities when moving towards the structural high (Fig. 3C). The maximum thickness reached by Unit IV in the Sines Drift area is less than 100 m (Fig. 5D). Strong reflections and minor internal erosional surfaces are also visible in the Sagres Drift area, where Unit IV is *ca* 250 m thick (Figs 4B and 5D). In deeper waters, Unit IV is *ca* 100 m thick in the northern part of the Infante Don Henrique Basin, while it is almost 200 m thick moving towards the footwall of the Marquês de Pombal Fault (Fig. 5D). The main depocentre in the area is located in the Marquês de Pombal Plateau, on the slope north-west of the SVC, where Unit IV consists of more than 450 m of sediment (Figs 3B, 4B and 5D). In this area, the reflections show higher amplitude compared to the older units. A significant number of seismically chaotic bodies are distributed within this unit in the MPP between 1.5 s and 2.0 s TWTT (Figs 3B and 4B). Unit IV displays an internal unconformity within the MPP area (Fig. 4B). Below this surface, the reflections are almost parallel to the underlying LQD, while above the unconformity reflections display onlap to the east and downlap to the west (Fig. 3B). In agreement with the observed internal geometries, Unit IV thins away from the

centre of the MPP and pinches out over structural highs located in both deep (below 3 s TWTT, Marquês de Pombal Fault hanging wall block) and shallow water settings (above 1.8 s TWTT, structural high south of the Sines Drift) (Fig. 3B).

Sedimentation rates

Overall, the decompacted sedimentation rates increase in the area through time by a factor of four or five. Unit I deposited in 0.9 Myr and the resulting sedimentation rates for the decompacted unit remain lower than 0.5 m kyr^{-1} along the entire study area (Fig. 6A). Similar sediment accumulation rates characterize Unit II (Fig. 6B), where sediment deposited during a longer time period (1.3 Myr). Nevertheless, sedimentation on both slopes adjacent to the SVC display comparatively higher accumulation rates than the underlying unit. Sedimentation rates significantly increase in the two uppermost units. Unit III, which deposited during 0.5 Myr, displays values exceeding 1.0 m kyr^{-1} on both sides of the SVC and in the deeper parts of the basin (Fig. 6C), and approximately 0.5 m kyr^{-1} are found in the Sines Drift. The highest decompacted sedimentation rates throughout the studied interval are found in Unit IV (Fig. 6D), which deposited in only 0.3 Myr. In this unit, sedimentation rates are lower than 0.3 m kyr^{-1} in the Sines Drift and in the northern part of the Infante Don Henrique Basin, while values up to 1.0 m kyr^{-1} are found at the foot of the Marquês de Pombal Fault and in the Sagres Drift. The highest sedimentation rates are found on the slope north-west of the SVC, where they exceed 2 m kyr^{-1} (Fig. 6D). Near seafloor sedimentation rates determined from multicore MC1 show values of 0.81 ± 0.07 m kyr^{-1} (Garcia-Orellana *et al.*, 2006) while the mean sedimentation rates at the same location provided by the stratigraphic interpretations are 1.1 m kyr^{-1}. Both of these sedimentation rates are within similar range and represent a relatively high value for a deep-sea setting.

Near-seafloor sediment characteristics

The sediments collected and analyzed for this study (Table 1; Figs 1 and 7) show a relatively homogenous grain size in all cores. MSCL P-wave velocity in core SdG083-13 (236 cm long), located in the shallowest part of the Marquês de Pombal Plateau, on a peripheral position with respect to the depocentre of Unit IV (Figs 5B, 6B and 7) ranges between 1455 ms^{-1} and 1555 ms^{-1}, with a visible increase recorded between 91 cm and 106 cm (Fig. 7A). Density increases from 1.61 g cm^{-3} in the shallower sediments to 2.02 g cm^{-3} in the deeper parts (porosities of 63% to 38% assuming a grain density of 2.65 g cm^{-3}), with an increase of the recorded P-wave velocity in the same interval (Fig. 7A). The anomalous interval does not find an expression in the grain-size distribution, which is homogeneous through the core. The core is silt-dominated (4 μm < Ø < 63 μm) along the whole length (between 57.3% and 73.29%), with slightly higher percentages of clay (Ø < 4 μm) in the shallower part (>40% above 70 cm) and more prevalent presence of sand (Ø > 63 μm) (between 2.5% and 4.7%) in the interval between 50 cm and 75 cm (Fig. 7A and E; see also Appendix S1). The mean grain size throughout the core is 8.6 μm.

Gravity cores SdG063-01 (243 cm), SdG063-02 (215 cm) and SdG063-03 (248 cm) were collected beyond the pinch-out of Unit IV (Figs 1, 3 and 7). P-wave velocity in core SdG063-01 ranges between 1590 ms^{-1} and 1633 ms^{-1}, while density increases linearly from 1.42 to 1.60 g cm^{-3} (porosity of 75% to 58%) (Fig. 7B). Two grain-size measurements from 180 to 195 cm interval record clay percentages between 33.85% and 37.71%, silt between 62.58% and 57.36%, and sand between 3.57% and 4.93% (Fig. 7B and E). Gravity cores SdG063-02 (Figs 1 and 7C) and SdG063-03 (Figs 1 and 7D) were collected 1.15 km away from one another. Core SdG063-02 was taken from inside a landslide scar (Minning *et al.*, 2006; Vizcaino *et al.*, 2006), while SdG063-03 comes from the undisturbed sediment above the landslide. SdG063-02 (Fig. 7C) shows P-wave velocity ranging between 1617 ms^{-1} and 1653 ms^{-1}, increasing below 207 cm of depth. Density varies between 1.56 g cm^{-3} (porosity 66%) and 1.73 g cm^{-3} (porosity 56%) (Fig. 7C). Grain size of the shallower interval sampled (78 to 110 cm depth) is mainly silt (61.26 to 62.95%), while in the deeper interval (207 to 217 cm) there is a higher percentage of sand (8.49%) with 66.23% silt and 25.28% clay (Fig. 7C and E). The MSCL measurements from core SdG063-03 resulted in a P-wave velocity between 1592 and 1625 ms^{-1}, while density increase linearly from 1.40 g cm^{-3} (porosity 75%) to 1.66 g cm^{-3} (porosity 60%) (Fig. 7D). The homogeneous grain-size composition of the core reflects the linear trend of the

logs: the uppermost sampled interval (133 to 148 cm) is mainly composed of silt (69.89 to 70.32%), with a minor percentage of clay (29.41 to 28.02%) and sand traces (0.70 to 1.66%). The deeper interval (240 cm to 248 cm) shows a similar composition, with 65.46% silt, 34.54% clay and no sand (Fig. 7D and E). All sediments sampled are poorly to very poorly sorted and strongly fine-skewed.

The IODP Site U1391 (Figs 1 and 3) recovered several sand rich intervals within Unit IV (Fig. 3D). Nevertheless, the two uppermost smear slide measurements (at 0.08 m and 0.9 m depth) resulted in clay-dominated sediments (between 65 and 70%) with high percentages of silt (20 to 27%) and sand between 3% and 5%. Starting from 2.6 m depth, the sand fraction increases (15%), reaching percentages up to 55% at 50 m depth. Multiple sand-rich layers are also present in Unit III, with sand beds attaining values of 65 to 70%, in Unit II and in Unit I (Fig. 3D). Finally, the bulk mineral composition of the 20 cm long multicore MC1 (Table 1, Fig. 1), shows that sediment is composed mainly by clay minerals (40 to 65%), and significant amounts of calcite (15 to 30%) and quartz (10 to 20%) (Garcia-Orellana *et al.*, 2006). Feldspar (<5%) and dolomite (<5%) were also present. The fraction coarser than 5 μm resulted in higher amounts of quartz (25 to 45%), feldspars (5 to 20%) and dolomite (<10%).

DISCUSSION

Down-slope versus along-slope processes in the Marquês de Pombal Plateau: significance of Units I to IV

Internal geometries and reflection characteristics of Units I to IV are interpreted as the result of the interplay between the predominant sedimentary processes in the area and their relative importance through time. In shallow areas, such as the Sines (Fig. 3C) and Sagres drifts (Fig. 4B) all four Plio-Quaternary units are the expression of contourite sedimentation controlled by the MOW hydrodynamics. Relatively high amplitude reflections show multiple channels, truncation and sediment waves, indicating high-contour current energy conditions (Figs 3C and 4B). This observation agrees with multiple sand layers, hiatuses and erosional features identified at IODP Site U1391 (Fig. 3D), which have been interpreted as variations in the MOW hydrodynamic regime (Hernández-Molina *et al.*, 2002; Llave *et al.*, 2006, 2007a; Brackenridge *et al.*, 2013; Stow *et al.*, 2013; Lofi *et al.*, 2016). Present-day water velocity data in these areas (up to 0.3 ms^{-1}) (Figs 3A and 4A; Appendix S1), indicate relatively strong bottom currents that would be able to transport the sediments found over the MPP (57 to 73% silt dominance) (Miller *et al.*, 1977; McCave, 1984) (Fig. 7E).

The transition from contourite sedimentation in the upper slope to that of deeper waters is, however, not so well understood. Beyond 1500 m water depth, bottom currents are relatively weak (*ca* 0.05 ms^{-1}) (Figs 3A and 4A) but thick sedimentary bodies with characteristics compatible with sediment transport by bottom currents are present. In this regard, the MCS profiles here presented (Figs 1, 3 and 4) offer a unique opportunity to image this transition and its interaction with a major sediment pathway such as the SVC. In the MPP, there is an overall upward increase in amplitude of seismic reflections and a change in seismic facies, which likely indicates the passage from a relatively homogeneous hemipelagic dominated sedimentation into a more energetic environment with increasing abundance of sandier and silty beds (Fig. 3B). This passage is concomitant with development of the SVC, which is mainly Quaternary (Serra *et al.*, 2020). Units I, II and III show parallel configuration of the reflections, without the clear erosive features that characterize the shallower part of the slope (Fig. 3B). Minor discontinuities are only visible within Units II and III from the perspective provided by profile BS09 (Fig. 4B). This change in stratal architecture is interpreted as the transition from a basinal lower-energy environment to a MOW-dominated deposition.

Unit IV displays pinch-out both upslope and downslope, accompanied by downlap (at 2.9 to 3.0 s TWTT; *ca* 2200 mbsl) (Fig. 3B) and onlap of internal reflections (at *ca* 2.5 s TWTT; *ca* 1800 m water depth), respectively. The sediments collected in water depths ranging from 2600 to 1000 m (within and outside the present depth range of the MOW) all show homogeneous poorly sorted clayey silts (Fig. 7). All of these features are diagnostic of contour current-related sedimentation (Faugères & Stow, 2008; Nielsen, Knutz, & Kuijpers, 2008; Nichols *et al.*, 2020). Further to that, Unit IV hosts the main depocentre in the study area, exceeding 450 m thick in its central part and a decompacted sedimentation rate of 2 m kyr^{-1} (Figs 3B, 4B, 5D and 6D), which is interpreted as the result of boosted sediment supply and significant turbidity current activity along the

SVC. In the Sagres Drift, south-east side of the canyon, Unit IV is *ca* 250 m thick, approximately half of the thickness in the MPP, resulting in an asymmetrical build-up of the slopes adjacent to the canyon (Figs 4B and 5D).

Contour currents are well-known to interact with turbidity currents and deposit their finer fraction downstream from the current (Rebesco *et al.*, 1996; Rasmussen *et al.*, 2003; Lucchi & Rebesco, 2007; Gong *et al.*, 2013; Edwards *et al.*, 2018; Fuhrmann *et al.*, 2020). Accordingly, this sedimentary body is interpreted as a mixed turbidite–contourite deep water drift, that has been named 'Marquês de Pombal Drift' (Fig. 7). Nevertheless, it should be noted here that the canyon is incised *ca* 1.5 km in the continental slope and that turbidity currents therefore travel deeply entrenched, making the interaction with contour currents more complex (see *Mechanisms of interaction between the Mediterranean Outflow Water and sediment gravity flows along the São Vicente Canyon* section for mechanisms facilitating interaction).

In shallow areas of the MPP, Units III and IV display sediment waves and stratal pinch-out features (Fig. 3B). These sediment waves extend in water depths between 950 m and 1650 m. A slightly undulated seafloor can be found down to water depths of 1850 m (Fig. 3B). The slope-parallel orientation of the wave crest suggests sediment mobilization perpendicular to the slope (Wynn & Stow, 2002; Ribó *et al.*, 2016). Similar features in 300 to 500 m water depth have been mapped, some kilometres eastward (Mestdagh *et al.*, 2020) and have been interpreted to result from internal wave energy propagating at the interface between the MOW and the AIW. Because of the depth at which sediment waves develop within Unit IV in the Marquês de Pombal Drift, those have most likely developed by internal waves propagating in between the base of the MOW and the underlying NADW (Fig. 8).

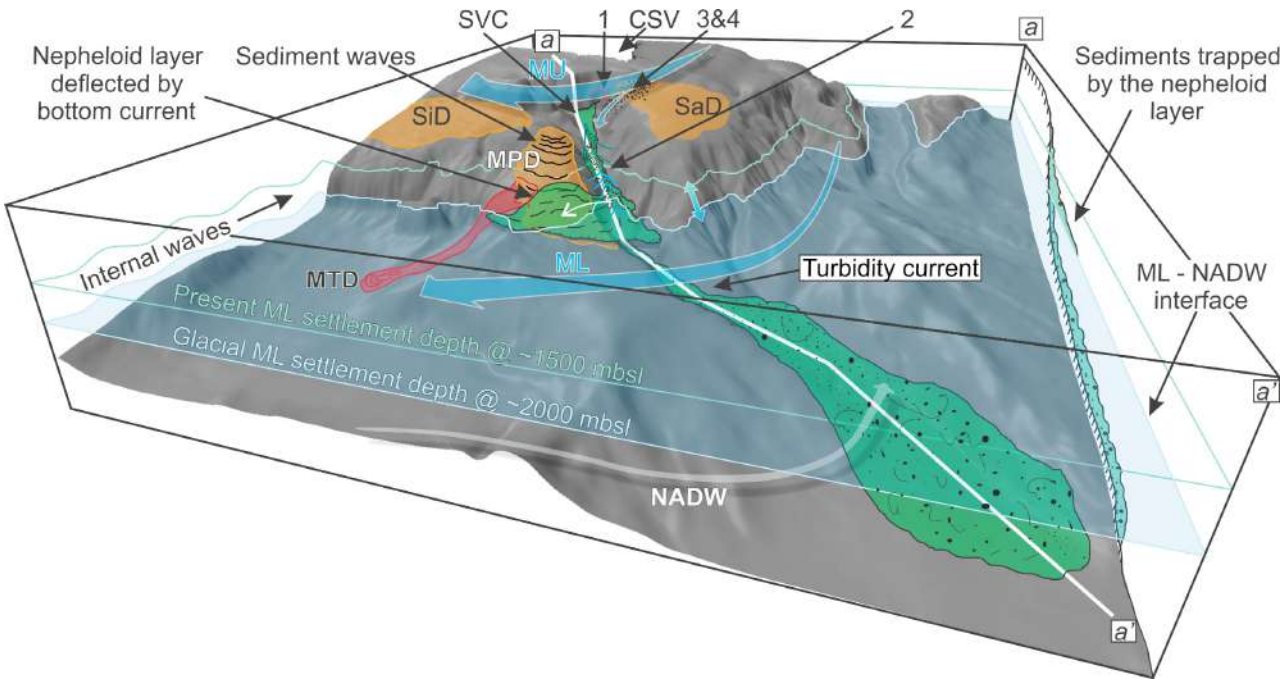

Fig. 8. Schematic representation of potential types of indirect interaction between the Mediterranean Outflow Water (MOW) and the sediment travelling along the São Vicente Canyon displayed during a glacial period. 1: Classical turbidity currents; 2: internal waves trapped in the canyon inducing sediment resuspension; 3: the denser lower part of the MOW upper core (MU) sinks in the canyon and rejoins ML at its neutral buoyancy level; 4: the MU entrains sediment in suspension, the near-bed water column gains density and sinks in the canyon. All of the scenarios require the formation of a nepheloid layer between the MOW and NADW along which the sediment finer fraction detached from the bottom of the canyon is incorporated in the MOW lower core (ML). White line along *a–a'* displays 2D section of sediment gravity flow and intermediate nepheloid layer on the side of the block diagram. CSV: Cape São Vicente; MPD: Marquês de Pombal Drift; SaD: Sagres Drift; SiD: Sines Drift; SVC: São Vicente Canyon; MU: MOW upper core; ML: MOW lower core; NADW: North Atlantic Deep Waters.

Faster sediment accumulation upsequence translates into a number of slope failures within Units III and IV in the Marquês de Pombal Drift, which display as chaotic lenses, interpreted as MTDs (Fig. 3B). Distribution of MTDs indicates that mass-wasting activity has been particularly intense during periods of erosion/non-deposition linked to enhancement and deepening of the MOW. A similar pattern of occurrence of MTDs has been reported in drifts of the eastern Gulf of Cadiz, such as the Lagos, Portimão (Fig. 1) and Faro drifts (Mulder *et al.*, 2003, 2006; Marchès *et al.*, 2010).

Multiple studies suggest that the main MOW core flows, at present, above 1500 m water depth along the northern part of the Gulf of Cadiz (Stow *et al.*, 1986; Mulder *et al.*, 2003; Llave *et al.*, 2007b, 2011; Hanquiez *et al.*, 2010; Hernández-Molina *et al.*, 2014b; Lofi *et al.*, 2016). Present day water velocity data (Figs 3A and 4A; Appendix S1) show that, at depths greater than 1900 m (2.4 s TWTT), the water current speed is as low as 0.03 ms^{-1}, which is only one-tenth of the speed reached in the shallower Sines or Sagres Drift areas (Figs 3A and 4A). The transport capacity of such slow bottom currents is not enough to transport the type of sediments found in the MPP (Fig. 7). However, the ML is estimated to settle in 2000 m water depth during glacial periods (Schönfeld & Zahn, 2000; Schönfeld *et al.*, 2003; Rogerson *et al.*, 2012a,b) (Fig. 8), resulting in enhancement of bottom currents over the MPP. Under these conditions, the MOW is capable of transporting sediment along most of the MPP. Enhancement and deepening of the ML also resulted in an increasing number of erosion/non-deposition events and changes in reflection configuration (parallel to slightly wavy and onlaps) (Figs 3B and 4B). This trend is probably linked to the longer duration and increased amplitude of sea-level oscillations after the Mid-Pleistocene Transition (Zachos *et al.*, 2001; Miller *et al.*, 2005; Clark *et al.*, 2006). The erosion/non-deposition horizons indicate that current velocities could intermittently exceed the value of 0.2 ms^{-1}, that marks the switch from depositional to erosional behavior of the ML (Stow *et al.*, 2009).

Mechanisms of interaction between the Mediterranean Outflow Water and sediment gravity flows along the São Vicente Canyon

The position of the late Quaternary deposit right on the slope north-west of the SVC, downstream from the MOW current orientation, suggests that interaction between sediment gravity flows within the canyon and the MOW could be responsible for its deposition. The retrogressive erosion that led to the incision of the SVC upper sector (Fig. 1) is also coeval with deposition of Unit IV (Serra *et al.*, 2020). Such retrogressive erosion triggered intense turbidity current activity that discharged sediments from the shallower part downslope, as confirmed by compositional analysis of piston cores collected in the Horseshoe Abyssal Plain (Lebreiro *et al.*, 1997). This activity continues to present, as sand and gravel deposits imaged in TOBI sidescan sonar data along the canyon thalweg (Vizcaino *et al.*, 2006; Serra *et al.*, 2020) indicate active sediment transport. Turbidity current activity within the canyon is also demonstrated by erosive bedforms such as grooves and scours, implying a minimum current speed between 1.0 and 2.5 ms^{-1} (Serra *et al.*, 2020).

The question that remains is nevertheless how the MOW can incorporate sediment from turbidity currents that travel within a canyon such as the SVC incised up to 1.5 km within the continental slope. The height of the canyon flanks clearly exceeds the maximum height of sediments brought to suspension by any observed turbidity current (Liu *et al.*, 2012; Azpiroz-Zabala *et al.*, 2017; Paull *et al.*, 2018), which typically do not exceed a few hundred metres. In the absence of hydrographic transects with measurements of suspended sediment concentration and/or time-series of moored sensors, several mechanisms by which sediment travelling along the SVC could be incorporated in the ML and Marquês de Pombal Drift afterwards are envisioned. All of these mechanisms require a density contrast in between water masses, here namely the MOW and NADW, along which a nepheloid layer can form with the finer sediment fraction detaching from the bottom of the canyon (de Stigter *et al.*, 2011; Ribó *et al.*, 2013) (Fig. 8):

First is the occurrence of classical turbidity currents within the canyon, where the most dilute part of the flow, upon encountering the density contrast in between the MOW and NADW, would form a nepheloid layer spreading out of the canyon and incorporated in the ML. Evidence of nepheloid layers associated with the MOW has been found further north on the Lisbon–Setúbal Canyon (de Stigter *et al.*, 2011) (Fig. 8).

Second, the strong density gradients at the boundaries of the MOW are thought to favour internal wave activity and sediment resuspension (McCave & Hall, 2002). It is well-known that submarine canyons trap internal wave energy, which drives elevated turbulence and mixing (e.g. Kunze *et al.*, 2002; Puig *et al.*, 2004). Re-suspended sediment could be temporarily incorporated into the ML and redeposited in the Marquês de Pombal Drift (Fig. 8).

Third, most works assume that the MU is geostrophically balanced at present. However, Ochoa & Bray (1991) and Marchès *et al.* (2007) report that several branches flow down small local canyons and eventually rejoin the main branch halfway to Cape São Vicente. Schönfeld & Zahn (2000) report increased MOW density during glacial maxima and periods of intensified MU extending to 1200 m water depth. If the flow (or the lower part of it) had (or still has) some density-driven component near the SVC, ageostrophic effects could be important. Hence, part of the MU (likely the denser lower part) could sink into the canyon and rejoin the lower core at its neutral buoyancy level (Fig. 8).

Fourth, if the MU is primarily geostrophic, but is able to entrain enough sediment in suspension, the potential exists for the near-bed water column to gain density and sink into the canyon. Given the lack of major fluvial inputs around Cape São Vicente, sediment supply to the MU mostly results from processes in the benthic boundary layer and have a significant seasonal component. Because the head of the SVC is located a mere 10 km from the coast and 200 m below sea level, on the MOW pathway (Fig. 1), it is likely that the MU could be trapped in the canyon given the last two hypotheses (Fig. 8). Fonnesu *et al.* (2020), Fuhrmann *et al.* (2020) and Miramontes *et al.* (2020) show that contour currents can winnow the finer part of a turbidity suspension cloud. In the model presented here, the interaction between turbidity currents travelling along the SVC and the MOW is mediated by a nepheloid layer, with the suspended sediment being deflected towards the north-west side of the canyon, downstream from the MOW, and ultimately deposited at the top of the Marquês de Pombal Drift (Figs 8 and 9).

Evidence linking the turbidity currents travelling along the SVC and the Marquês de Pombal Drift is provided by the dolomite present in the terrigenous fraction of the sediments collected from the drift (Garcia-Orellana *et al.*, 2006) (Fig. 1). At IODP Site U1391, dolomite rich sediments were recovered from Units I and II, as dolomite diagenesis was associated with depositional hiatuses during the LPD and EQD (IODP Expedition 339 Scientists, 2013b; Hernández-Molina *et al.*, 2016a). The stratigraphic

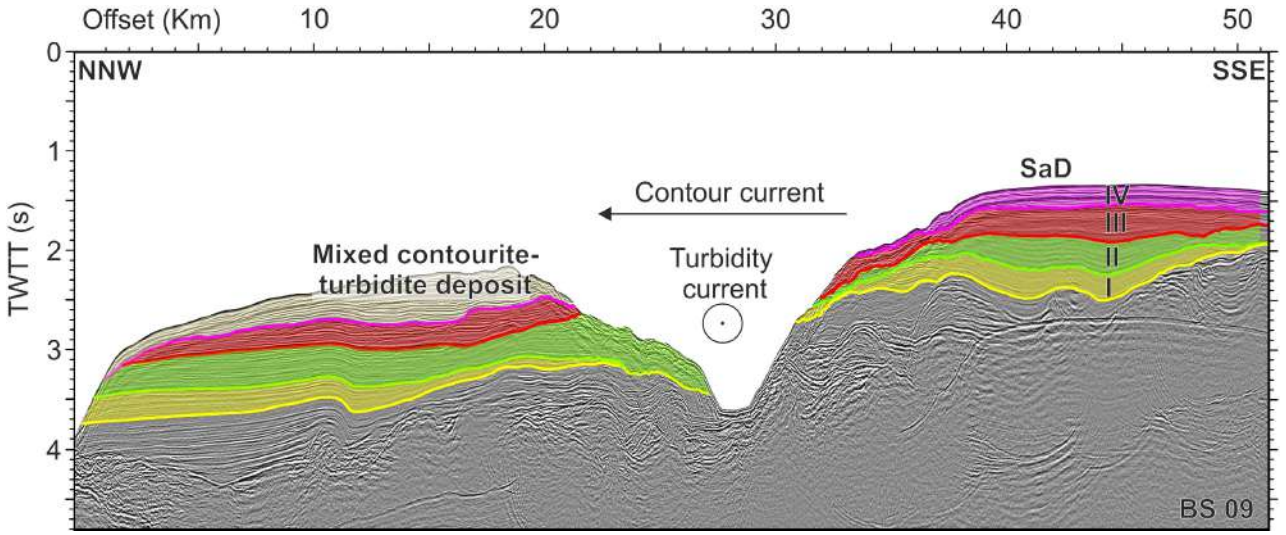

Fig. 9. Interpreted cross-section of the São Vicente Canyon from multi-channel seismic profile BS09 (see location in Fig. 1) showing position and size of the drift deposit generated by the mixed turbidite – contourite system. I, II, III and IV correspond to the different units defined in this study; SaD: Sagres Drift; SVC: São Vicente Canyon; vertical exaggeration *ca* 4; TWTT: two-way travel time.

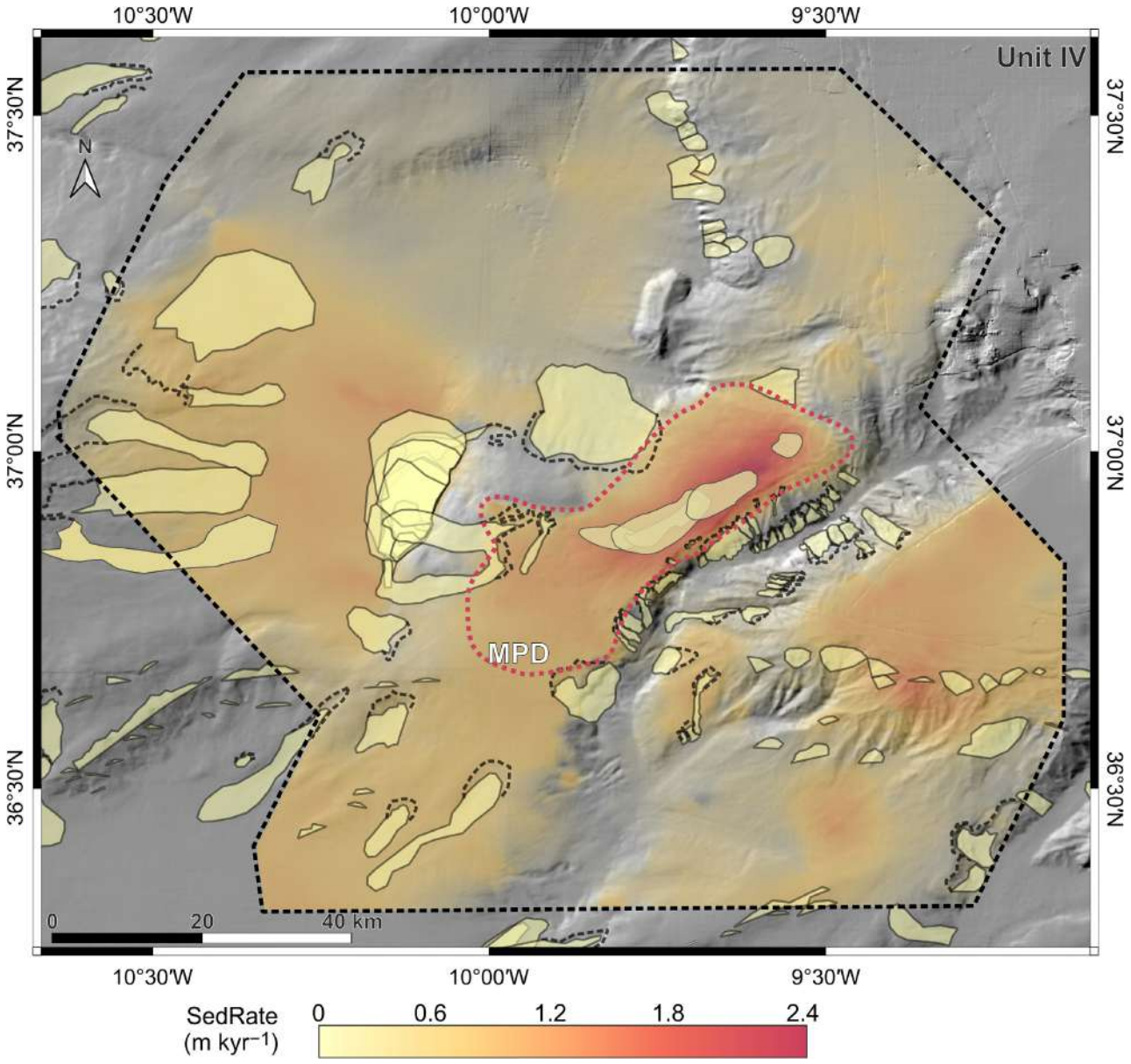

Fig. 10. Location and size of mass transport deposits (MTDs) and scars within the area of interest plotted together with sedimentation rates of the Late Quaternary Unit IV. Red dashed outline shows the approximate areal distribution of the Marquês de Pombal Drift (MPD).

interpretation of the area reveals that Units I and II in the Alentejo Basin are exposed only at the head and flanks of the SVC, where erosion reaches the early Pliocene (Fig. 4B). Thus, mineral composition indicates that the sediments at the top of the late Quaternary Marquês de Pombal Drift belong to older stratigraphic units (Units I and II), eroded during the canyon formation.

Features diagnostic of mixed turbidite–contourite systems such as regular uni-directional, low-angle, offset stacking of channels and lobe complexes (Fonnesu *et al.*, 2020; Fuhrmann *et al.*, 2020) and smooth slopes upstream of the bottom current (Rebesco *et al.*, 1996) are not found in the mixed turbidite – contourite system of the Marquês de Pombal Drift. The steep slope of the northern flank of the SVC (Fig. 4) is rather

a result of intense erosional processes along the canyon, while its position is locked within a syncline between two major thrust faults (Serra *et al.*, 2020). Mixed turbidite – contourite depositional systems developing in channel–levée systems have been widely recognized (Rebesco *et al.*, 1996; Michels *et al.*, 2001; Gong *et al.*, 2013; He *et al.*, 2013; Hernández-Molina *et al.*, 2016b; Sansom, 2018; Fonnesu *et al.*, 2020). However, in all previous cases, direct interaction between turbidity currents and contour currents was made possible because the incision was not deep, allowing turbidity current overbanking with consequent migration of the channels upstream from the contour current (e.g. Gong *et al.*, 2013; Fuhrmann *et al.*, 2020).

The morphological and depositional differences found in between the Marquês de Pombal Drift and those of previous studies might require introducing a new mixed turbidite – contourite depositional model. While previously mentioned studies refer to syn-depositional interaction within the turbidity currents, this case is better described as a syn-erosional to syn-depositional interaction between turbidity currents affecting submarine canyons and contour currents. In this model, contour currents capture the finer-grained component of turbidity currents within submarine canyons via nepheloid layers and deposit this sediment on the slope adjacent to the canyon downstream from the contour current.

Flume tank experiments (e.g. Cossu *et al.*, 2010, 2015) and direct observations (e.g. Peakall *et al.*, 2012) show that the Coriolis force may also have a significant influence in asymmetrical deposition within levées in channel–levée systems, especially at high latitudes. Asymmetrical deposition in these levées departs from the assumption that the levée height provides an indication of the flow depth (Bowen *et al.*, 1984). However, given that the SVC is incised to a depth of between 1000 m and 1500 m in the depth range of the Marquês de Pombal Drift, turbidity currents along the canyon are likely to be fully contained within the canyon. Therefore, it seems unlikely that the Coriolis force alone could have a significant role in the development of the Marquês de Pombal Drift.

Significance for submarine slope instability

Numerous MTDs are evident both within the Marquês de Pombal Drift and around its perimeter (Figs 2 and 10). There are several stacked MTDs in the Infante Don Henrique Basin, which translates into a relatively thick sequence in this basin and high accumulation rates (Figs 5 and 6). Most of these MTDs that accumulate in the Infante Don Henrique Basin originate from the MPP (Fig. 2). The relatively high seismicity in the area (Stich *et al.*, 2005; Martínez-Loriente *et al.*, 2013, 2018) suggests that earthquake shaking likely played a major role in the observed slope failures. However, the very high sedimentation rates (up to 2 m kyr^{-1}) (Fig. 6D), large lateral variations in thickness (Figs 3B and 5D) and fine particle size, usually associated with low permeability, that constitute the Marquês de Pombal Drift (Fig. 7) may have had a significant influence in overpressure build-up of the underlying units (Urgeles *et al.*, 2010; Dugan & Sheahan, 2012; Urlaub *et al.*, 2015; Llopart *et al.*, 2019; Sammartini *et al.*, 2019; Mencaroni *et al.*, 2020). Hydrogeological models that consider the mechanical/hydrodynamic properties of the mixed turbidite – contourite system and its architecture as described in this work would enable the quantification of excess pore pressure build-up.

CONCLUSIONS

Seismic data and sediment cores reveal the existence of a >450 m thick, silt-dominated sedimentary body on the slope north-west of the São Vicente Canyon (SVC), which was largely deposited during the late Quaternary in concurrent development with the canyon. Sedimentation rates in this sedimentary body increased steadily from the late Pliocene to the late Quaternary, from values not exceeding 0.2 m kyr^{-1} to values up to 2.0 m kyr^{-1}. The sedimentary body is interpreted as the result of a mixed downslope–alongslope sedimentary system generated from interaction of the Mediterranean Outflow Water (MOW) with turbidity currents travelling along the São Vicente Canyon and has been named the 'Marquês de Pombal Drift'. Part of the drift morphology is also the result of sediment remobilization by internal waves. The deeper parts of this drift are likely active only during glacial periods when the MOW settles deeper, as present conditions are not favourable for transport of the grain-size fraction present over the drift. The peculiarity of this mixed turbidite–contourite system, with respect to previously reported mixed systems, is that it develops adjacent to a canyon the incision of which (up to

1.5 km) exceeds the height of turbidity currents by several hundred metres, thus direct interaction between down-slope and along-slope currents is unlikely to take place. Several mechanisms by which sediment travelling along the SVC could be incorporated in the MOW can be hypothesized. All of these mechanisms require a density contrast in between water masses, here namely the MOW and North Atlantic Deep Water (NADW), along which a nepheloid layer can form with the sediment finer fraction detaching from the bottom of the canyon: (i) classical turbidity currents; (ii) sediment resuspension from internal waves trapped within the canyon; (iii) trapping of part of the MU and sinking in the canyon, particularly when the MOW is denser (for example, glacial periods); and (vi) entrainment of sediment at the base of the MOW upper core (MU) providing additional density to the flow for it to sink into the SVC. In all cases, the coarser particle fraction within the flow would settle in the canyon, while the finer sediments from an intermediate nepheloid layer would be incorporated in the deeper MOW core (ML). These finer sediments are finally deposited on the north-west slope of the canyon, originating the mixed turbidite–contourite sedimentary body. The presence of multiple mass transport deposits (MTDs) distributed around the Marquês de Pombal Drift suggests that high accumulation rates of fine-grained sediment is at the origin of excess pore pressure build-up and failure initiation.

Bottom currents worldwide are linked to water masses that offer density contrasts along which nepheloid layers can form. Therefore, the depositional dynamics reposted in this study could potentially take place in other canyons crossing the path of a contour current. Because submarine canyons are the major sediment pathway in most continental margins, the sedimentary processes described in this study could have a significant role in along-slope sediment transport worldwide.

ACKNOWLEDGEMENTS

We thank the captains, crews and science parties of the INSIGHT Leg1 and Leg2 cruises onboard *R/V Sarmiento de Gamboa*. We are grateful to reviewers S. de Castro, U. Nicholson and E. Miramontes for their valuable suggestions and constructive reviews that greatly improved the manuscript. This research received funding by the European Union's Horizon 2020 research and innovating programme under the Marie Sklodowska-Curie grant via project ITN-SLATE (grant agreement No 721403). The Spanish "Ministerio de Ciencia e Innovación" and the European Regional Development Fund are also acknowledged for funding through grant CTM2015-70155-R (project INSIGHT). This research used samples and data provided by the International Ocean Discovery Program (IODP). This study has used data from the E.U. Copernicus Marine Service Information.

DATA AVAILABILITY STATEMENT

The data that support the findings of this study are available from the corresponding author upon reasonable request.

REFERENCES

Alonso, B., **Ercilla, G.**, **Casas, D.**, **Stow, D.A.V.**, **Rodríguez-Tovar, F.J.**, **Dorador, J.** and **Hernández-Molina, F.J.** (2016) Contourite vs gravity-flow deposits of the Pleistocene Faro Drift (Gulf of Cadiz): Sedimentological and mineralogical approaches. *Mar. Geol.*, **377**, 77–94.

Ambar, I. and **Howe, M.R.** (1979) Observations of the Mediterranean outflow-I mixing in the Mediterranean outflow. *Deep Sea Res. Part A. Oceanogr. Res. Pap.*, **26**, 535–554.

Ambar, I., **Howe, M.R.** and **Abdullah, M.I.**(1976) A physical and chemical description of the mediterranean outflow in the Gulf of Cadiz. *Dtsch. Hydrogr. Z.*, **29**, 58–68.

Amo, A., **Reffray, G.**, **Sotillo, M.G.**, **Aznar, R.** and **Guihou, K.** (2020) Atlantic -Iberian Biscay Irish- Ocean Physics Analysis and Forecast Product: IBI_ANALYSIS_FORECAST_PHYS_005_001. Prod. User Man. (7.0), 1–45. https://resources.marine.copernicus.eu/documents/PUM/CMEMS-IBI-PUM-005-001.pdf.

Azpiroz-Zabala, M., **Cartigny, M.J.B.**, **Talling, P.J.**, **Parsons, D.R.**, **Sumner, E.J.**, **Clare, M.A.**, **Simmons, S.M.**, **Cooper, C.** and **Pope, E.L.** (2017) Newly recognized turbidity current structure can explain prolonged flushing of submarine canyons. *Sci. Adv.*, **3**, e1700200. https://doi.org/10.1126/sciadv.1700200

Bahr, A., **Kaboth, S.**, **Jiménez-Espejo, F.J.**, **Sierro, F.J.**, **Voelker, A.H.L.**, **Lourens, L.**, **Röhl, U.**, **Reichart, G.J.**, **Escutia, C.**, **Hernández-Molina, F.J.**, **Pross, J.** and **Friedrich, O.** (2015) Persistent monsoonal forcing of mediterranean outflow water dynamics during the late Pleistocene. *Geology*, **43**, 951–954.

Baptista, M.A. and **Miranda, J.M.** (2009) Revision of the portuguese catalog of tsunamis. *Nat. Hazards Earth Syst. Sci.*, **9**, 25–42.

Baringer, M.O. and **Price, J.F.** (2002) Mixing and Spreading of the Mediterranean Outflow. *J. Phys. Oceanogr.*, **27**, 1654–1677.

Bartolome, R., **Gràcia, E.**, **Stich, D.**, **Martínez-Loriente, S.**, **Klaeschen, D.**, **de Lis Mancilla, F.**, **Lo Iacono, C.**,

Dañobeitia, J.J. and **Zitellini, N.** (2012) Evidence for active strike-slip faulting along the Eurasia-Africa convergence zone: Implications for seismic hazard in the southwest Iberian margin. *Geology*, **40**, 495–498.

Bowen, A.J., **Normark, W.R.** and **Piper, D.J.W.** (1984) Modelling of turbidity currents on Navy Submarine Fan, California Continental Borderland. *Sedimentology*, **31**, 169–185.

Brackenridge, R.E., **Hernández-Molina, F.J.**, **Stow, D.A.V.** and **Llave, E.** (2013) A Pliocene mixed contourite-turbidite system offshore the Algarve Margin, Gulf of Cadiz: Seismic response, margin evolution and reservoir implications. *Mar. Pet. Geol.*, **46**, 36–50.

Brackenridge, R.E., **Stow, D.A.V.**, **Hernández-Molina, F.J.**, **Jones, C.**, **Mena, A.**, **Alejo, I.**, **Ducassou, E.**, **Llave, E.**, **Ercilla, G.**, **Nombela, M.A.**, **Perez-Arlucea, M.** and **Frances, G.** (2018) Textural characteristics and facies of sand-rich contourite depositional systems. *Sedimentology*, **65**, 2223–2252.

Cacho, I., **Grimalt, J.O.**, **Sierro, F.J.**, **Shackleton, N.** and **Canals, M.** (2000) Evidence for enhanced Mediterranean thermohaline circulation during rapid climatic coolings. *Earth Planet. Sci. Lett.*, **183**, 417–429.

Camerlenghi, A., **Rebesco, M.** and **Pudsey, C.J.** (1997) High Resolution Terrigenous Sedimentary Record of a Sediment Drift on the Antarctic Peninsula Pacific Margin (Initial Results of the "SEDANO" Program). In: *The Antarctic Region: Geological Evolution and Processes* (Ed. Ricci, C. A.). Siena, Terra Antarctica Pubblication, 705–710.

Casas, D., **Casalbore, D.**, **Yenes, M.** and **Urgeles, R.** (2015) Submarine mass movements around the iberian Peninsula. The building of continental margins through hazardous processes. *Bol. Geol. y Min.*, **126**, 257–278.

de Castro, S., **Hernández-Molina, F.J.**, **Rodríguez-Tovar, F.J.**, **Llave, E.**, **Ng, Z.L.**, **Nishida, N.** and **Mena, A.** (2020) Contourites and bottom current reworked sands: Bed facies model and implications. *Mar. Geol.*, **428**, 106267. https://doi.org/10.1016/j.margeo.2020.106267.

Clark, P.U., **Archer, D.**, **Pollard, D.**, **Blum, J.D.**, **Rial, J.A.**, **Brovkin, V.**, **Mix, A.C.**, **Pisias, N.G.** and **Roy, M.** (2006) The middle Pleistocene transition: characteristics, mechanisms, and implications for long-term changes in atmospheric pCO2. *Quat. Sci. Rev.*, **25**, 3150–3184.

Cossu, F.R., **Wells, M.G.** and **Peakall, J.** (2015) Latitudinal variations in submarine channel sedimentation patterns: The role of coriolis forces. *J. Geol. Soc. London.*, **172**, 161–174.

Cossu, R., **Wells, M.G.** and **Whlin, A.K.** (2010) Influence of the coriolis force on the velocity structure of gravity currents in straight submarine channel systems. *J. Geophys. Res. Ocean.*, **115**, 1–15.

Dugan, B. and **Sheahan, T.C.** (2012) Offshore sediment overpressures of passive margins: Mechanisms, measurement, and models. *Rev. Geophys.*, **50**, 271–276.

Edwards, C., **McQuaid, S.**, **Easton, S.**, **Scott, D.**, **Couch, A.**, **Evans, R.** and **Hart, S.** (2018) Lateral accretion in a straight slope channel system: An example from the Forties Sandstone of the Huntington Field, UK Central North Sea. *Pet. Geol. Conf. Proc.*, **8**, 413–428.

Escutia, C., **Nelson, C.H.**, **Acton, G.D.**, **Eittreim, S.L.**, **Cooper, A.K.**, **Warnke, D.A.** and **Jaramillo, J.M.** (2002) Current controlled deposition on the Wilkes Land continental rise. *Antarctica. Geol. Soc. Mem.*, **22**, 373–384.

Faugères, J.C. and **Stow, D.A.V.** (2008) Contourite drifts: nature, evolution and controls. In: *Developments in Sedimentology. Contourites.* (Eds Rebesco, M. and Camerlenghi, A.). Amsterdam: Elsevier, **60**, 257–288. https://doi.org/10.1016/S0070-4571(08)10014-0

Fonnesu, M., **Palermo, D.**, **Galbiati, M.**, **Marchesini, M.**, **Bonamini, E.** and **Bendias, D.** (2020) A new world-class deep-water play-type, deposited by the syndepositional interaction of turbidity flows and bottom currents: The giant Eocene Coral Field in northern Mozambique. *Mar. Pet. Geol.*, **111**, 179–201.

Ford, J., **Urgeles, R.**, **Camerlenghi, A.** and **Gràcia, E.** (2021) Seismic diffraction imaging to characterise mass-transport complexes: examples from the Gulf of Cadiz, south west Iberian Margin. *J. Geophys. Res. Solid Earth*, **126**, e2020JB021474. http://dx.doi.org/10.1029/2020jb021474.

Frigola, J., **Canals, M.** and **Mata, P.** (2015) Techniques for the non-destructive and continuous analysis of sediment cores. Application in the Iberian continental margin. *Bol. Geol. y Min.*, **126**, 609–634.

Fuhrmann, A., **Kane, I.A.**, **Clare, M.A.**, **Ferguson, R.A.**, **Schomacker, E.**, **Bonamini, E.** and **Contreras, F.A.** (2020) Hybrid turbidite-drift channel complexes: An integrated multiscale model. *Geology*, **48**, 562–568.

Garcia-Orellana, J., **Gràcia, E.**, **Vizcaino, A.**, **Masqué, P.**, **Olid, C.**, **Martínez-Ruiz, F.**, **Piñero, E.**, **Sanchez-Cabeza, J.A.** and **Dañobeitia, J.** (2006) Identifying instrumental and historical earthquake records in the SW Iberian margin 210Pb turbidite chronology. *Geophys. Res. Lett.*, **33**, L24601. https://doi.org/10.1029/2006GL028417

Gong, C., **Wang, Y.**, **Zhu, W.**, **Li, W.** and **Xu, Q.** (2013) Upper Miocene to Quaternary unidirectionally migrating deep-water channels in the Pearl River Mouth Basin, northern South China Sea. *Am. Assoc. Pet. Geol. Bull.*, **97**, 285–308.

Gong, C., **Wang, Y.**, **Rebesco, M.**, **Salon, S.** and **Steel, R.J.** (2018) How do turbidity flows interact with contour currents in unidirectionally migrating deep-water channels? *Geology*, **46**, 551–554.

Gràcia, E., **Danobeitia, J.** and **Vergés, J.** (2003a) Mapping active faults offshore Portugal (36 Њ N – 38 Њ N): Implications for seismic hazard assessment along the southwest Iberian margin. *Geology*, **31**, 83–86.

Gràcia, E., **Dañobeitia, J.**, **Vergés, J.**, **Bartolomé, R.** and **Córdoba, D.** (2003b) Crustal architecture and tectonic evolution of the Gulf of Cadiz (SW Iberian margin) at the convergence of the Eurasian and African plates. *Tectonics*, **22**, 1033–1056.

Gràcia, E., **Vizcaino, A.**, **Escutia, C.**, **Asioli, A.**, **Rodés, Á.**, **Pallàs, R.**, **Garcia-Orellana, J.**, **Lebreiro, S.** and **Goldfinger, C.** (2010) Holocene earthquake record offshore Portugal (SW Iberia): testing turbidite paleoseismology in a slow-convergence margin. *Quat. Sci. Rev.*, **29**, 1156–1172.

Grützner, J., **Rebesco, M.A.**, **Cooper, A.K.**, **Forsberg, C.F.**, **Kryc, K.A.** and **Wefer, G.** (2003) Evidence for orbitally controlled size variations of the East Antarctic Ice Sheet during the late Miocene. *Geology*, **31**, 777–780.

Hanquiez, V., **Mulder, T.**, **Lecroart, P.**, **Gonthier, E.**, **Marchès, E.** and **Voisset, M.** (2007) High resolution seafloor images in the Gulf of Cadiz, Iberian margin. *Mar. Geol.*, **246**, 42–59.

Hanquiez, V., **Mulder, T.**, **Toucanne, S.**, **Lecroart, P.**, **Bonnel, C.**, **Marchès, E.** and **Gonthier, E.** (2010) The sandy channel-lobe depositional systems in the Gulf of Cadiz: Gravity processes forced by contour current processes. *Sediment. Geol.*, **229**, 110–123.

He, Y., **Xie, X.**, **Kneller, B.C.**, **Wang, Z.** and **Li, X.** (2013) Architecture and controlling factors of canyon fills on the

shelf margin in the Qiongdongnan Basin, northern South China Sea. *Mar. Pet. Geol.*, **41**, 264–276.

Hernández-Molina, F.J., **Llave, E.**, **Preu, B.**, **Ercilla, G.**, **Fontan, A.**, **Bruno, M.**, **Serra, N.**, **Gomiz, J.J.**, **Brackenridge, R.E.**, **Sierro, F.J.**, **Stow, D.A.V.**, **García, M.**, **Juan, C.**, **Sandoval, N.** and **Arnaiz, A.** (2014a) Contourite processes associated with the Mediterranean Outfl ow Water after its exit from the Strait of Gibraltar: Global and conceptual implications. *Geology*, **42**, 227–230.

Hernández-Molina, F.J., **Serra, N.**, **Stow, D.A.V.**, **Llave, E.**, **Ercilla, G.** and **van Rooij, D.** (2011) Along-slope oceanographic processes and sedimentary products around the Iberian margin. *Geo-Marine Lett.*, **31**, 315–341.

Hernández-Molina, F.J., **Sierro, F.J.**, **Llave, E.**, **Roque, C.**, **Stow, D.A.V.**, **Williams, T.**, **Lofi, J.**, **Van der Schee, M.**, **Arnáiz, A.**, **Ledesma, S.**, **Rosales, C.**, **Rodríguez-Tovar, F.J.**, **Pardo-Igúzquiza, E.** and **Brackenridge, R.E.** (2016a) Evolution of the gulf of Cadiz margin and southwest Portugal contourite depositional system: Tectonic, sedimentary and paleoceanographic implications from IODP expedition 339. *Mar. Geol.*, **377**, 7–39.

Hernández-Molina, F.J., **Somoza, L.**, **Vazquez, J.T.**, **Lobo, F.**, **Fernández-Puga, M.C.**, **Llave, E.** and **Díaz-del Río, V.** (2002) Quaternary stratigraphic stacking patterns on the continental shelves of the southern Iberian Peninsula: Their relationship with global climate and palaeoceanographic changes. *Quat. Int.*, **92**, 5–23.

Hernández-Molina, F.J., **Soto, M.**, **Piola, A.R.**, **Tomasini, J.**, **Preu, B.**, **Thompson, P.**, **Badalini, G.**, **Creaser, A.**, **Violante, R.A.**, **Morales, E.**, **Paterlini, M.** and **De Santa Ana, H.** (2016b) A contourite depositional system along the Uruguayan continental margin: Sedimentary, oceanographic and paleoceanographic implications. *Mar. Geol.*, **378**, 333–349.

Hernández-Molina, F.J., **Stow, D.A.V.**, **Alvarez-Zarikian, C.A.**, **Acton, G.**, **Bahr, A.**, **Balestra, B.**, **Ducassou, E.** and **Flood, R.** (2014b) Onset of Mediterranean outflow into the North Atlantic. *Science*, **344**, 1244–1250.

IODP Expedition 339 Scientists (2013a) Expedition 339 summary. In: *Proc. IODP* (Eds Stow, D.A.V., Hernández-Molina, F.J., Alvarez Zarikian, C.A., and the Expedition 339 Scientists), Integrated Ocean Drilling Program Management International, Inc., Tokyo, **339**. https://doi.org/10.2204/iodp.proc.339.101.2013

IODP Expedition 339 Scientists (2013b) Site U1391 - Visual core description. In: *Proc. IODP* (Eds Stow, D.A.V., Hernández-Molina, F.J., Alvarez Zarikian, C.A., and the Expedition 339 Scientists), Integrated Ocean Drilling Program Management International, Inc., Tokyo, **339**. https://doi.org/10.2204/iodp.proc.339.109.2013.

IODP Expedition 339 Scientists (2013c) Site U1391 - Smear slides. In: *Proc. IODP* (Eds Stow, D.A.V., Hernández-Molina, F.J., Alvarez Zarikian, C.A., and the Expedition 339 Scientists), Integrated Ocean Drilling Program Management International, Inc., Tokyo, **339**. https://doi.org/10.2204/iodp.proc.339.109.2013.

Jiménez-Espejo, F.J., **Pardos-Gené, M.**, **Martínez-Ruiz, F.**, **García-Alix, A.**, **van de Flierdt, T.**, **Toyofuku, T.**, **Bahr, A.** and **Kreissig, K.** (2015) Geochemical evidence for intermediate water circulation in the westernmost Mediterranean over the last 20kyrBP and its impact on the Mediterranean Outflow. *Glob. Planet. Change*, **135**, 38–46.

Johnson, J., **Ambar, I.**, **Serra, N.** and **Stevens, I.** (2002) Comparative studies of the spreading of Mediterranean Water through the Gulf of Cadiz. *Deep. Res. Part II Top. Stud. Oceanogr.*, **49**, 4179–4193.

Kane, I.A., **Kane, I.A.**, **Clare, M.A.**, **Miramontes, E.**, **Wogelius, R.**, **Rothwell, J.J.**, **Garreau, P.** and **Pohl, F.** (2020) Seafloor microplastic hotspots controlled by deep-sea circulation. *Science*, **80**, 1–11.

Knutz, P.C. (2008) Chapter 24 Palaeoceanographic significance of contourite drifts. *Dev. Sedimentol.*, **60**, 511–535.

Kunze, E., **Rosenfeld, L.K.**, **Carter, G.S.** and **Gregg, M.C.** (2002) Internal waves in Monterey Submarine Canyon. *J. Phys. Oceanogr.*, **32**, 1890–1913.

Laberg, J.S. and **Camerlenghi, A.** (2008) The Significance of Contourites for Submarine Slope Stability. *Develop. Sedimentol.*, **60**, 537–556.

Laberg, J.S., **Stoker, M.S.**, **Dahlgren, K.I.T.**, **de Haas, H.**, **Haflidason, H.**, **Hjelstuen, B.O.**, **Nielsen, T.**, **Shannon, P.M.**, **Vorren, T.O.**, **van Weering, T.C.E.** and **Ceramicola, S.** (2005) Cenozoic alongslope processes and sedimentation on the NW European Atlantic margin. *Mar. Pet. Geol.*, **22**, 1069–1088.

Lebreiro, S.M., **Mccave, N.I.** and **Weaver, P.P.E.** (1997) Late Quaternary Turbidite Emplacement on the Horseshoe Abyssal Plain (Iberian Margin). *SEPM J. Sediment. Res.*, **67**, 856–870. https://doi.org/10.1306/d4268658-2b26-11d7-8648000102c1865d

Liu, J.T., **Wang, Y.H.**, **Yang, R.J.**, **Hsu, R.T.**, **Kao, S.J.**, **Lin, H.L.** and **Kuo, F.H.** (2012) Cyclone-induced hyperpycnal turbidity currents in a submarine canyon. *J. Geophys. Res. Ocean.*, **117**, 1–12.

Llave, E., **Hernández-molina, F.J.**, **Somoza, L.**, **Stow, D.A.V.**, **Díaz Del Río, V.**, **Mar, D.C.**, **Vigo, U.D.** and **Southampton, S.** (2007a) Quaternary evolution of the contourite depositional system in the Gulf of Cadiz. *Geol. Soc. Spec. Publ.*, **276**, 49–79.

Llave, E., **Hernández-Molina, F.J.**, **Stow, D.A.V.**, **Fernández-Puga, M.C.**, **García, M.**, **Vázquez, J.T.**, **Maestro, A.**, **Somoza, L.** and **Díaz del Río, V.** (2007b) Reconstructions of the Mediterranean Outflow Water during the quaternary based on the study of changes in buried mounded drift stacking pattern in the Gulf of Cadiz. *Mar. Geophys. Res.*, **28**, 379–394.

Llave, E., **Hernández-Molina, F.J.**, **García, M.**, **Ercilla, G.**, **Roque, C.**, **Juan, C.**, **Mena, A.**, **Preu, B.**, **Van Rooij, D.**, **Rebesco, M.**, **Brackenridge, R.**, **Jané, G.**, **Gómez-Ballesteros, M.** and **Stow, D.** (2019) Contourites along the Iberian continental margins: conceptual and economic implications. SP476-2017-46 pp.

Llave, E., **Matias, H.**, **Hernández-Molina, F.J.**, **Ercilla, G.**, **Stow, D.A.V.** and **Medialdea, T.** (2011) Pliocene-Quaternary contourites along the northern Gulf of Cadiz margin: Sedimentary stacking pattern and regional distribution. *Geo-Marine Lett.*, **31**, 377–390.

Llave, E., **Schönfeld, J.**, **Hernández-Molina, F.J.**, **Mulder, T.**, **Somoza, L.**, **Díaz Del Río, V.** and **Sánchez-Almazo, I.** (2006) High-resolution stratigraphy of the Mediterranean outflow contourite system in the Gulf of Cadiz during the late Pleistocene: The impact of Heinrich events. *Mar. Geol.*, **227**, 241–262.

Llopart, J., **Urgeles, R.**, **Forsberg, C.F.**, **Camerlenghi, A.**, **Vanneste, M.**, **Rebesco, M.**, **Lucchi, R.G.**, **Rüther, D.C.** and **Lantzsch, H.** (2019) Fluid flow and pore pressure development throughout the evolution of a trough mouth fan, western Barents Sea. *Basin Res.*, **31**, 487–513.

Lo Iacono, C., **Gràcia, E.**, **Zaniboni, F.**, **Pagnoni, G.**, **Tinti, S.**, **Bartolomé, R.**, **Masson, D.G.**, **Wynn, R.B.**, **Lourenccedil, N.**, **de Abreu, M.P.**, **Dañobeitia, J.J.** and **Zitellini, N.** (2012) Large, deepwater slope failures: Implications for landslide-generated tsunamis. *Geology*, **40**, 931–934.

Lofi, J., **Voelker, A.H.L.**, **Ducassou, E.**, **Hernández-Molina, F.J.**, **Sierro, F.J.**, **Bahr, A.**, **Galvani, A.**, **Lourens, L.J.**, **Pardo-Igúzquiza, E.**, **Pezard, P.**, **Rodríguez-Tovar, F.J.** and **Williams, T.** (2016) Quaternary chronostratigraphic framework and sedimentary processes for the Gulf of Cadiz and Portuguese Contourite Depositional Systems derived from Natural Gamma Ray records. *Mar. Geol.*, **377**, 40–57.

Lucchi, R.G. and **Rebesco, M.** (2007) Glacial contourites on the Antarctic Peninsula margin: Insight for palaeoenvironmental and palaeoclimatic conditions. *Geol. Soc. Spec. Publ.*, **276**, 111–127.

Marchès, E., **Mulder, T.**, **Cremer, M.**, **Bonnel, C.**, **Hanquiez, V.**, **Gonthier, E.** and **Lecroart, P.** (2007) Contourite drift construction influenced by capture of Mediterranean Outflow Water deep-sea current by the Portimão submarine canyon (Gulf of Cadiz, South Portugal). *Mar. Geol.*, **242**, 247–260.

Marchès, E., **Mulder, T.**, **Gonthier, E.**, **Cremer, M.**, **Hanquiez, V.**, **Garlan, T.** and **Lecroart, P.** (2010) Perched lobe formation in the Gulf of Cadiz: Interactions between gravity processes and contour currents (Algarve Margin, Southern Portugal). *Sediment. Geol.*, **229**, 81–94.

Martínez-Loriente, S., **Gràcia, E.**, **Bartolome, R.**, **Sallarès, V.**, **Connors, C.**, **Perea, H.**, **Lo Iacono, C.**, **Klaeschen, D.**, **Terrinha, P.**, **Dañobeitia, J.J.** and **Zitellini, N.** (2013) Active deformation in old oceanic lithosphere and significance for earthquake hazard: Seismic imaging of the Coral Patch Ridge area and neighboring abyssal plains (SW Iberian Margin). *Geochem. Geophys. Geosystems*, **14**, 2206–2231.

Martínez-Loriente, S., **Gràcia, E.**, **Bartolome, R.**, **Perea, H.**, **Klaeschen, D.**, **Dañobeitia, J.J.**, **Zitellini, N.**, **Wynn, R.B.** and **Masson, D.G.** (2018) Morphostructure, tectono-sedimentary evolution and seismic potential of the Horseshoe Fault. *SW Iberian Margin. Basin Res.*, **30**, 382–400.

McCave, I.N. (1984) Erosion, transport and deposition of fine-grained marine sediments. *Geol. Soc. Spec. Publ.*, **15**, 35–69.

McCave, I.N. and **Hall, I.R.** (2002) Turbidity of waters over the Northwest Iberian continental margin. *Prog. Oceanogr.*, **52**, 299–313.

Mencaroni, D., **Llopart, J.**, **Urgeles, R.**, **Lafuerza, S.**, **Gràcia, E.**, **Le Friant, A.** and **Urlaub, M.** (2020) From gravity cores to overpressure history: the importance of measured sediment physical properties in hydrogeological models. *Geol. Soc., London, Spec. Public.*, **500**(1), 289–300.

Mestdagh, T., **Lobo, F.J.**, **Llave, E.**, **Hernández-Molina, F.J.** and **Van Rooij, D.** (2019) Review of the late Quaternary stratigraphy of the northern Gulf of Cadiz continental margin: New insights into controlling factors and global implications. *Earth-Science Rev.*, **198**, 102944.

Mestdagh, T., **Lobo, F.J.**, **Llave, E.**, **Hernández-Molina, F.J.**, **García Ledesma, A.**, **Puga-Bernabéu, Á.**, **Fernández-Salas, L.M.** and **Rooij, D.V.** (2020) Late Quaternary multi-genetic processes and products on the northern Gulf of Cadiz upper continental slope (SW Iberian Peninsula). *Mar. Geol.*, **427**, 106214.

Michels, K.H., **Kuhn, G.**, **Hillenbrand, C.D.**, **Diekmann, B.**, **FÜtterer, D.K.**, **Grobe, H.** and **Uenzelmann-Neben, G.**(2002) The southern Weddell Sea: combined contourite-turbidite sedimentation at the southeastern margin of the Weddell Gyre. *Geol. Soc. Mem.*, **22**, 305–323.

Michels, K.H., **Rogenhagen, J.** and **Kuhn, G.** (2001) Recognition of contour-current influence in mixed contourite-turbidite sequences of the western Weddell Sea, Antarctica. *Mar. Geophys. Res.*, **22**, 465–485.

Miller, K.G., **Kominz, M.A.**, **Browning, J.V.**, **Wright, J.D.**, **Mountain, G.S.**, **Katz, M.E.**, **Sugarman, P.J.**, **Cramer, B.S.**, **Christie-Blick, N.** and **Pekar, S.F.** (2005) The phanerozoic record of global sea-level change. *Science*, **310**, 1293–1298.

Miller, M.C., **McCave, I.N.** and **Komar, P.D.** (1977) Threshold of Sediment Motion under Unidirectional Currents. *Sedimentology*, **24**, 507–527.

Minning, M., **Hebbeln, D.**, **Hensen, C.** and **Kopf, A.** (2006) Geotechnical and geochemical investigations of the Marquês de Pombal landslide at the Portuguese continental margin. *Nor. Geol. Tidsskr.*, **86**, 187–198.

Miramontes, E., **Cattaneo, A.**, **Jouet, G.** and **Garziglia, S.** (2016a) Implications of sediment dynamics in mass transport along the Pianosa Ridge (Northern Tyrrhenian Sea). *Adv. Nat. Technol. Hazards Res.*, **41**, 301–309.

Miramontes, E., **Cattaneo, A.**, **Jouet, G.**, **Théreau, E.**, **Thomas, Y.**, **Rovere, M.**, **Cauquil, E.** and **Trincardi, F.** (2016b) The Pianosa Contourite Depositional System (Northern Tyrrhenian Sea): Drift morphology and Plio-Quaternary stratigraphic evolution. *Mar. Geol.*, **378**, 20–42.

Miramontes, E., **Eggenhuisen, J.T.**, **Silva Jacinto, R.**, **Poneti, G.**, **Pohl, F.**, **Normandeau, A.**, **Campbell, D.C.** and **Hernández-Molina, F.J.** (2020) Channel-levee evolution in combined contour current–turbidity current flows from flume-tank experiments. *Geology*, **48**, 353–357.

Miramontes, E., **Garreau, P.**, **Caillaud, M.**, **Jouet, G.**, **Pellen, R.**, **Hernández-Molina, F.J.**, **Clare, M.A.** and **Cattaneo, A.** (2019) Contourite distribution and bottom currents in the NW Mediterranean Sea: Coupling seafloor geomorphology and hydrodynamic modelling. *Geomorphology*, **333**, 43–60.

Miramontes, E., **Garziglia, S.**, **Sultan, N.**, **Jouet, G.** and **Cattaneo, A.** (2018) Morphological control of slope instability in contourites: a geotechnical approach. *Landslides*, **15**, 1085–1095.

Mulder, T., **Faugères, J.C.** and **Gonthier, E.** (2008) Mixed turbidite-contourite systems. *Dev. Sedimentol.*, **60**, 435–456.

Mulder, T., **Lecroart, P.**, **Hanquiez, V.**, **Marches, E.**, **Gonthier, E.**, **Guedes, J.C.**, **Thiébot, E.**, **Jaaidi, B.**, **Kenyon, N.**, **Voisset, M.**, **Perez, C.**, **Sayago, M.**, **Fuchey, Y.** and **Bujan, S.** (2006) The western part of the Gulf of Cadiz: Contour currents and turbidity currents interactions. *Geo-Marine Lett.*, **26**, 31–41.

Mulder, T., **Voisset, M.**, **Lecroart, P.**, **Le Drezen, E.**, **Gonthier, E.**, **Hanquiez, V.**, **Faugres, J.C.**, **Habgood, E.**, **Hernández-Molina, F.J.**, **Estrada, F.**, **Llave-Barranco, E.**, **Poirier, D.**, **Gorini, C.**, **Fuchey, Y.**, **Voelker, A.**, **Freitas, P.**, **Sanchez, F.L.**, **Fernandez, L.M.**, **Kenyon, N.H.**, **Morel, J.**, **Hernandez-Molina, F.J.**, **Estrada, F.**, **Llave-Barranco, E.**, **Poirier, D.**, **Gorini, C.**, **Fuchey, Y.**, **Voelker, A.**, **Freitas, P.**, **Sanchez, F.L.**, **Fernandez, L.M.**, **Kenyon, N.H.** and **Morel, J.** (2003) The Gulf of Cadiz: an unstable giant contouritic levee. *Geo-Marine Lett.*, **23**, 7–18.

Nelson, C.H., **Baraza, J.**, **Maldonado, A.**, **Rodero, J.**, **Escutia, C.** and **Barber, J.H.** (1999) Influence of the Atlantic inflow

and Mediterranean outflow currents on Late Quaternary sedimentary facies of the Gulf of Cadiz continental margin. *Mar. Geol.*, **155**, 99–129.

Nichols, M.D., **Xuan, C.**, **Crowhurst, S.**, **Hodell, D.A.**, **Richter, C.**, **Acton, G.D.** and **Wilson, P.A.** (2020) Climate-Induced Variability in Mediterranean Outflow to the North Atlantic Ocean During the Late Pleistocene. *Paleoceanogr. Paleoclimatology*, **35**, 1–17.

Nicholson, U., **Libby, S.**, **Tappin, D.R.** and **McCarthy, D.** (2020) The Subantarctic Front as a sedimentary conveyor belt for tsunamigenic submarine landslides. *Mar. Geol.*, **424**, 106161.

Nielsen, T., **Knutz, P.C.** and **Kuijpers, A.** (2008) Chapter 16 seismic expression of contourite depositional systems. *Dev. Sedimentol.*, **60**, 301–321.

Ochoa, J. and **Bray, N.A.** (1991) Water mass exchange in the Gulf of Cadiz. *Deep Sea Res. Part A. Oceanogr. Res. Pap.*, **38**, S465–S503.

Paull, C.K., **Talling, P.J.**, **Maier, K.L.**, **Parsons, D.**, **Xu, J.**, **Caress, D.W.**, **Gwiazda, R.**, **Lundsten, E.M.**, **Anderson, K.**, **Barry, J.P.**, **Chaffey, M.**, **O'Reilly, T.**, **Rosenberger, K.J.**, **Gales, J.A.**, **Kieft, B.**, **McGann, M.**, **Simmons, S.M.**, **McCann, M.**, **Sumner, E.J.**, **Clare, M.A.** and **Cartigny, M.J.** (2018) Powerful turbidity currents driven by dense basal layers. *Nat. Commun.*, **9**, 1–9.

Peakall, J., **Kane, I.A.**, **Masson, D.G.**, **Keevil, G.**, **Mccaffrey, W.** and **Corney, R.** (2012) Global (latitudinal) variation in submarine channel sinuosity. *Geology*, **40**, 11–14.

Puig, P., **Palanques, A.**, **Guillén, J.** and **El Khatab, M.** (2004) Role of internal waves in the generation of nepheloid layers on the northwestern Alboran slope: Implications for continental margin shaping. *J. Geophys. Res. C Ocean.*, **109**, 1–11.

Rasmussen, S., **Lykke-Andersen, H.**, **Kuijpers, A.** and **Troelstra, S.R.** (2003) Post-miocene sedimentation at the continental rise of Southeast Greenland: The interplay between turbidity and contour currents. *Mar. Geol.*, **196**, 37–52.

Rebesco, M. and **Camerlenghi, A.** (Eds) (2006) *Contourites*. Elsevier, Amsterdam, 666 pp.

Rebesco, M., **Camerlenghi, A.**, **Volpi, V.**, **Neagu, C.**, **Accettella, D.**, **Lindberg, B.**, **Cova, A.**, **Zgur, F.** and **Party, M.** (2007) Interaction of processes and importance of contourites: Insights from the detailed morphology of sediment Drift 7. *Antarctica. Geol. Soc. Spec. Publ.*, **276**, 95–110.

Rebesco, M. and **Camerlenghi, A.** (2008) Late Pliocene margin development and mega debris flow deposits on the Antarctic continental margins: Evidence of the onset of the modern Antarctic Ice Sheet? *Palaeogeogr. Palaeoclimatol. Palaeoecol.*, **260**, 149–167.

Rebesco, M., **Hernández-Molina, F.J.**, **Van Rooij, D.** and **Wåhlin, A.** (2014) Contourites and associated sediments controlled by deep-water circulation processes: State-of-the-art and future considerations. *Mar. Geol.*, **352**, 111–154.

Rebesco, M., **Larter, R.D.**, **Camerlenghi, A.** and **Barker, P.F.** (1996) Giant sediment drifts on the continental rise west of the Antarctic Peninsula. *Geo-Marine Lett.*, **16**, 65–75.

Ribó, M., **Puig, P.**, **Salat, J.** and **Palanques, A.** (2013) Nepheloid layer distribution in the Gulf of Valencia, northwestern Mediterranean. *J. Mar. Syst.*, **111–112**, 130–138.

Ribó, M., **Puig, P.**, **Muñoz, A.**, **Lo Iacono, C.**, **Masqué, P.**, **Palanques, A.**, **Acosta, J.**, **Guillén, J.** and **Gómez Ballesteros, M.** (2016) Morphobathymetric analysis of the large fine-grained sediment waves over the Gulf of Valencia continental slope (NW Mediterranean). *Geomorphology*, **253**, 22–37.

Rogerson, M., **Bigg, G.R.**, **Rohling, E.J.** and **Ramirez, J.** (2012a) Vertical density gradient in the eastern North Atlantic during the last 30,000 years. *Clim. Dyn.*, **39**, 589–598.

Rogerson, M., **Rohling, E.J.**, **Weaver, P.P.E.** and **Murray, J.W.** (2005) Glacial to interglacial changes in the settling depth of the Mediterranean Outflow plume. *Paleoceanography*, **20**, 1–12.

Rogerson, M., **Rohling, E.J.**, **Bigg, G.R.** and **Ramirez, J.** (2012b) Paleoceanography of the Atlantic-Mediterranean exchange: Overview and first quantitative assessment of climatic forcing. *Rev. Geophys*, **50**, RG2003. https://doi.org/10.1029/2011RG000376.

Sallarès, V., **Martínez-Loriente, S.**, **Prada, M.**, **Gràcia, E.**, **Ranero, C.**, **Gutscher, M.A.**, **Bartolome, R.**, **Gailler, A.**, **Dañobeitia, J.J.** and **Zitellini, N.** (2013) Seismic evidence of exhumed mantle rock basement at the Gorringe Bank and the adjacent Horseshoe and Tagus abyssal plains (SW Iberia). *Earth Planet. Sci. Lett.*, **365**, 120–131.

Sammartini, M., **Camerlenghi, A.**, **Budillon, F.**, **Insinga, D.D.**, **Zgur, F.**, **Conforti, A.**, **Iorio, M.**, **Romeo, R.** and **Tonielli, R.** (2019) Open-slope, translational submarine landslide in a tectonically active volcanic continental margin (Licosa submarine landslide, southern tyrrhenian sea). *Geol. Soc. Spec. Publ.*, **477**, 133–150.

Sánchez-Leal, R.F., **Bellanco, M.J.**, **Fernández-Salas, L.M.**, **García-Lafuente, J.**, **Gasser-Rubinat, M.**, **González-Pola, C.**, **Hernández-Molina, F.J.**, **Pelegrí, J.L.**, **Peliz, A.**, **Relvas, P.**, **Roque, D.**, **Ruiz-Villarreal, M.**, **Sammartino, S.** and **Sánchez-Garrido, J.C.** (2017) The mediterranean overflow in the Gulf of Cadiz: A rugged journey. *Sci. Adv.*, **3**, 1–12.

Sansom, P. (2018) Hybrid turbidite–contourite systems of the Tanzanian margin. *Pet. Geosci.*, **24**, 258–276.

Schönfeld, J. and **Zahn, R.** (2000) Late Glacial to Holocene history of the Mediterranean outflow. Evidence from benthic foraminiferal assemblages and stable isotopes at the Portuguese margin. *Palaeogeogr. Palaeoclimatol. Palaeoecol.*, **159**, 85–111.

Schönfeld, J., **Zahn, R.** and **De Abreu, L.** (2003) Surface and deep water response to rapid climate changes at the Western Iberian margin. *Glob. Planet. Change*, **36**, 237–264.

Serra, C.S., **Martínez-Loriente, S.**, **Gràcia, E.**, **Urgeles, R.**, **Vizcaino, A.**, **Perea, H.**, **Bartolome, R.**, **Pallàs, R.**, **Lo Iacono, C.**, **Diez, S.**, **Dañobeitia, J.**, **Terrinha, P.** and **Zitellini, N.** (2020) Tectonic evolution, geomorphology and influence of bottom currents along a large submarine canyon system: The São Vicente Canyon (SW Iberian margin). *Mar. Geol.*, **426**, 106219.

Serra, N., **Ambar, I.** and **Käse, R.H.** (2005) Observations and numerical modelling of the Mediterranean outflow splitting and eddy generation. *Deep. Res. Part II Top. Stud. Oceanogr.*, **52**, 383–408.

Shanmugam, G., **Spalding, T.D.** and **Rofheart, D.H.** (1993) Process sedimentology and reservoir quality of deep-marine bottom- current reworked sands (sandy contourites): an example from the Gulf of Mexico. *Am. Assoc. Pet. Geol. Bull.*, **77**, 1241–1259.

Silva, S., **Terrinha, P.**, **Matias, L.**, **Duarte, J.C.**, **Roque, C.**, **Ranero, C.R.**, **Geissler, W.H.** and **Zitellini, N.** (2017) Micro-seismicity in the Gulf of Cadiz: Is there a link

between micro-seismicity, high magnitude earthquakes and active faults? *Tectonophysics*, **717**, 226–241.

Solheim, A., **Berg, K.**, **Forsberg, C.F.** and **Bryn, P.** (2005) The Storegga Slide complex: Repetitive large scale sliding with similar cause and development. *Mar. Pet. Geol.*, **22**, 97–107.

Sotillo, M.G., **Cailleau, S.**, **Lorente, P.**, **Levier, B.**, **Aznar, R.**, **Reffray, G.**, **Amo-Baladrón, A.**, **Chanut, J.**, **Benkiran, M.** and **Alvarez-Fanjul, E.** (2015) The myocean IBI ocean forecast and reanalysis systems: Operational products and roadmap to the future copernicus service. *J. Oper. Oceanogr.*, **8**, 63–79.

Stich, D., **de Mancilla, F.L.** and **Morales, J.**(2005) Crust-mantle coupling in the Gulf of Cadiz (SW-Iberia). *Geophys. Res. Lett.*, **32**, 1–4.

Stich, D., **de Mancilla, F. L.**, **Pondrelli, S.** and **Morales, J.**(2007) Source analysis of the February 12th 2007, Mw 6.0 Horseshoe earthquake: Implications for the 1755 Lisbon earthquake. *Geophys. Res. Lett.*, **34**, L12308.

de Stigter, H.C., **Jesus, C.C.**, **Boer, W.**, **Richter, T.O.**, **Costa, A.** and **van Weering, T.C.E.** (2011) Recent sediment transport and deposition in the Lisbon-Setúbal and Cascais submarine canyons, Portuguese continental margin. *Deep. Res. Part II Top. Stud. Oceanogr.*, **58**, 2321–2344.

Stow, D.A.V., **Faugères, J.C.** and **Gonthier, E.** (1986) Facies distribution and textural variation in Faro Drift contourites: Velocity fluctuation and drift growth. *Mar. Geol.*, **72**, 71–100.

Stow, D.A.V., **Faugères, J.C.**, **Howe, J.A.**, **Pudsey, C.J.** and **Viana, A.R.** (2002) Bottom currents, contourites and deep-sea sediment drifts: Current state-of-the-art. *Geol. Soc. Mem.*, **22**, 7–20.

Stow, D.A.V., **Hernández-Molina, F.J.**, **Llave, E.**, **Sayago-Gil, M.**, **Díaz-del Río, V.** and **Branson, A.** (2009) Bedform-velocity matrix: The estimation of bottom current velocity from bedform observations. *Geology*, **37**, 327–330.

Stow, D.A.V., **Hernández-Molina, F.J.**, **Llave, E.**, **Bruno, M.**, **García, M.**, **Díaz del Rio, V.**, **Somoza, L.** and **Brackenridge, R.E.** (2013) The Cadiz Contourite Channel: Sandy contourites, bedforms and dynamic current interaction. *Mar. Geol.*, **343**, 99–114.

Terrinha, P., **Matias, L.**, **Vicente, J.**, **Duarte, J.**, **Luís, J.**, **Pinheiro, L.**, **Lourenço, N.**, **Diez, S.**, **Rosas, F.**, **Magalhães, V.**, **Valadares, V.**, **Zitellini, N.**, **Roque, C.** and **Víctor, L.M.** (2009) Morphotectonics and strain partitioning at the Iberia-Africa plate boundary from multibeam and seismic reflection data. *Mar. Geol.*, **267**, 156–174.

Terrinha, P., **Pinheiro, L.M.**, **Henriet, J.P.**, **Matias, L.**, **Ivanov, M.K.**, **Monteiro, J.H.**, **Akhmetzhanov, A.**, **Volkonskaya, A.**, **Cunha, T.**, **Shaskin, P.** and **Rovere, M.** (2003) Tsunamigenic-seismogenic structures, neotectonics, sedimentary processes and slope instability on the southwest Portuguese Margin. *Mar. Geol.*, **195**, 55–73.

Thorpe, S.A. (1975) Variability of the mediterranean undercurrent in the Gulf of Cadiz. *Deep Sea Res. Oceanogr. Abstr.*, **23**, 711-IN1.

Urgeles, R. and **Camerlenghi, A.** (2013) Submarine landslides of the Mediterranean Sea: Trigger mechanisms, dynamics, and frequency-magnitude distribution. *J. Geophys. Res. Earth Surf.*, **118**, 2600–2618.

Urgeles, R., **Locat, J.**, **Sawyer, D.E.**, **Flemings, P.B.**, **Dugan, B.** and **Binh, N.T.T.** (2010) History of Pore Pressure Build Up and Slope Instability in Mud-Dominated Sediments of Ursa Basin, Gulf of Mexico Continental Slope BT - Submarine Mass Movements and Their Consequences. In: *Submarine Mass Movements and Their Consequences* (Eds Mosher, D.C., Shipp, R.C., Moscardelli, L., Chaytor, J.D., Baxter, C.D.P., Lee, H.J. and Urgeles, R.), pp. 179–190.Springer, Dordrecht.

Urlaub, M., **Talling, P.J.**, **Zervos, A.** and **Masson, D.G.** (2015) What causes large submarine landslides on low gradient sediment accumulation ? *J. Geophys. Res. Solid Earth*, **120**, 1–18.

Van Hinte, J.E. (1978) Geohistory Analysis-Application of Micropaleontology in Exploration Geology. *Am. Assoc. Pet. Geol. Bull*, **62**, 201–222. https://doi.org/10.1306/c1ea4815-16c9-11d7-8645000102c1865d

Viana, A.R. and **Rebesco, M.** (2007) *Economic and Palaeoceanographic Significance of Contourite Deposits*. The Geological Society, London, 276 pp.

Vizcaino, A., **Gràcia, E.**, **Pallàs, R.**, **Garcia-Orellana, J.**, **Escutia, C.**, **Casas, D.**, **Willmott, V.**, **Diez, S.**, **Asioli, A.** and **Dañobeitia, J.** (2006) Sedimentology, physical properties and age of mass transport deposits associated with the Marquês de Pombal Fault, Southwest Portuguese Margin. *Nor. Geol. Tidsskr.*, **86**, 177–186.

Voelker, A.H.L., **Jimenez-Espejo, F.J.**, **Bahr, A.**, **Acton, G.D.**, **Rebotim, A.**, **Salgueiro, E.**, **Röhl, C.** and **Escutia, C.** (2014) Mediterranean Outflow Water changes in the Gulf of Cadiz during the Mid-Pleistocene transition — the role of insolation. In: *Book of Abstracts. 2nd Deep-Water Circulation Congress: The Contourite Log-book. Ghent, Belgium, 10–12 September 2014* (Eds van Rooij, D. and Rüggeberg, A.), VLIZ Special Publication, 69, Ghent University, Department of Geology and Soil Science — Flanders Marine Institute (VLIZ), Oostende, Belgium, **2014**, pp. 29-30.

Wentworth, C.K. (1922) A Scale of Grade and Class Terms for Clastic Sediments. *J. Geol.*, **30**, 377–392.

Wynn, R.B. and **Stow, D.A.V.** (2002) Classification and characterisation of deep-water sediment waves. *Mar. Geol.*, **192**, 7–22.

Yu, X., **Stow, D.**, **Smillie, Z.**, **Esentia, I.**, **Brackenridge, R.**, **Xie, X.**, **Bankole, S.**, **Ducassou, E.** and **Llave, E.** (2020) Contourite porosity, grain size and reservoir characteristics. *Mar. Pet. Geol.*, **117**, 104392.

Zachos, J., **Pagani, H.**, **Sloan, L.**, **Thomas, E.** and **Billups, K.** (2001) Trends, rhythms, and aberrations in global climate 65 Ma to present. *Science*, **292**, 686–693.

Zitellini, N., **Gràcia, E.**, **Matias, L.**, **Terrinha, P.**, **Abreu, M.A.**, **De Alteriis, G.**, **Henriet, J.P.**, **Dañobeitia, J.J.**, **Masson, D.G.**, **Mulder, T.**, **Ramella, R.**, **Somoza, L.** and **Diez, S.** (2009) The quest for the Africa-Eurasia plate boundary west of the Strait of Gibraltar. *Earth Planet. Sci. Lett.*, **280**, 13–50.

Zitellini, N., **Mendes, L.A.**, **Cordoba, D.**, **Danobeitia, J.**, **Nicolich, R.**, **Pellis, G.**, **Ribeiro, A.**, **Sartori, R.**, **Torelli, L.**, **Bartolome, R.**, **Bortoluzzi, G.**, **Calafato, A.**, **Carrilho, F.**, **Casoni, L.**, **Chierici, E.**, **Corela, C.**, **Correggiari, A.**, **Delia Vedova, B.**, **Gracia, E.**, **Jornet, P.**, **Landuzzi, M.**, **Ligi, M.**, **Magagnoli, A.**, **Marozzi, G.**, **Matias, L.**, **Penitenti, D.**, **Rodriguez, P.**, **Rovere, M.**, **Terrinha, P.**, **Vigliotti, L.** and **Ruiz, A.Z.** (2001) Source of 1755 lisbon earthquake and tsunami investigated. *Eos*, **82**, 285–291.

Zitellini, N., **Rovere, M.**, **Terrinha, P.**, **Chierici, F.**, **Matias, L.**, **Victor, L.M.**, **Corela, C.**, **Ribeiro, A.**, **Cordoba, D.**, **Danobeitia, J.J.**, **Grácia, E.**, **Bartolomé, R.**, **Nicolich, R.**, **Pellis, G.**, **Della Vedova, B.**, **Sartori, R.**, **Torelli, L.**, **Correggiari, A.** and **Vigliotii, L.** (2004) Neogene through

quaternary tectonic reactivation of SW Iberian passive margin. *Pure Appl. Geophys.*, **161**, 565–587.

Manuscript received 8 July 2020; revision 11 January 2021; revision accepted 18 January 2021

Supporting Information

Additional information may be found in the online version of this article:

Appendix S1: Fig. S1. Original water speed profiles related with MCS profiles Line 10 (A) and BS21 (B) (Fig. 1) (Amo *et al.*, 2020; Sotillo *et al.*, 2015).

Fig. S2. Original salinity profiles related with MCS profiles Line 10 (A) and BS21 (B) (Fig. 1) (Amo *et al.*, 2020; Sotillo *et al.*, 2015).

Table S1. Grain size distribution related with four gravity cores considered in this study.

